LAL 92–13
March 1992

Laboratoire de l'Accélérateur Linéaire

STUDY OF TEV RANGE COSMIC RAY DETECTION WITH CERENKOV IMAGING TECHNIQUES

R. Ansari, J.M. Gaillard, G. Parrour

Laboratoire de l'Accélérateur Linéaire, IN2P3-CNRS et Université de Paris-Sud, F-91405 Orsay Cedex, France

U.E.R
de
l'Université Paris-Sud

Institut National
de Physique Nucléaire
et
de Physique des Particules

Bâtiment 200 - 91405 ORSAY Cedex

LAL 92–13
March 1992

STUDY OF TeV RANGE COSMIC RAY DETECTION WITH CERENKOV IMAGING TECHNIQUES

R. Ansari, J.M. Gaillard, G. Parrour

Laboratoire de l'Accélérateur Linéaire, IN2P3-CNRS,
et Université de Paris-Sud, F-91405 Orsay Cedex, France

Contents

1 INTRODUCTION

The Monte Carlo study of cosmic ray detection in the TeV energy range presented in this paper has been triggered by our interest in the ARTEMIS (*A*ntimatter *R*esearch *T*hrough the *E*arth *M*oon *I*on *S*pectrometer) proposal. The concept of ARTEMIS to search for antimatter from other galaxies using the earth magnetic field to measure the sign of the charge and the moon as an absorber is due to M. Urban (LPNHE - Ecole Polytechnique). The ARTEMIS project is described in some detail in reference [1] and [2]. A brief presentation of the key ideas of Artemis is given in Appendix A.

A possibility has been found by M. Urban and his colleagues for a test of the Artemis concepts by using, with some modifications the existing mirror telescope of the Whipple Laboratory at Mount Hopkins (USA). We are not participating in that development. However the Monte Carlo study which had been started has been continued and is available as a tool for more general use. Our study deals with the properties of cosmic ray showers detected by Cerenkov imaging in the visible domain. The detection sensitivity and the accuracy of the reconstruction of the parent particle direction using Cerenkov imaging are discussed. The backbone of the study is the Monte Carlo generator developped by A.M. Hillas (University of Leeds). This work has been mainly done during the summer and fall 1990, and the beginning of 1991. But, due to various reasons, the preparation of the report has been delayed.

In section 2 a brief overview of cosmic ray detection methods and a description of the setup used for the simulations are given. The characteristics of the atmospheric shower Monte Carlo generator used in this study are presented in section 3. Section 4 is devoted to the discussion of shower characteristics with Cerenkov detection. A comparison between nucleon and photon induced showers is also included. Section 5 and 6 contain results on the reconstruction properties for the setup used in the simulation.

2 CERENKOV IMAGING FOR COSMIC RAY DETECTION

2.1 Detection Methods, an overview

A brief overview of cosmic ray detection technics is given here. A more complete discussion can be found in references [3], [4] and [5].

Cosmic ray particles produce a shower of secondary particles ($e^{\pm}$, γ, $\mu^{\pm}$, ν, $\pi^{\pm}$, π^{o}, ...) through nuclear collisions, and electron-photon cascades, in the earth atmosphere. Terrestrial detection uses the shower development effects. Three methods have been used up to now:

a) Cerenkov light is emitted by the charged particles (mainly electrons) produced in the shower. Cerenkov photons can be collected by large mirrors (few meters in diameter), equipped with amplifying photodetectors in the focal plane. Very low ambient light-level. (Dark night sky, without the moon) is required, given the low signal amplitude. The Cerenkov detection method is applicable for relatively low energy ($\sim$ 100 GeV) cosmic ray detection, and is widely used in the VHE (Very High Energy) 10^2 GeV $\rightarrow$ 10^2 TeV range. The number of collected Cerenkov photons, which is roughly proportional to the number of charged secondaries, can be used to estimate the initial parent energy. The well known timing method consisting of measuring the photons arrival time with several telescopes can be used for the parent direction determination. Cerenkov imaging provides an interesting alternative to this method.

b) A small fraction of the charged secondaries can reach the ground, depending on the parent particle direction and mainly its energy, as well as the observation site altitude.

High energy secondary particles keep a certain memory of the parent direction. Muons (μ^+, μ^-), mainly produced in charged pion ($\pi^{\pm} \rightarrow \mu^{\pm} + \nu_{\mu}$) decays in hadron initiated showers, have small multiple scattering cross-section. High energy muons can thus reach the ground with directions highly correlated with the parent direction. They can be used for the reconstruction of the initial direction of hadronic showers. Timing methods are also applicable to the direction measurements, while charged particle counting can be used for measuring the parent energy. Charged particle detection is used in the UHE (Ultra High Energy) range from 10^{11} eV(100 TeV) to 10^{17} eV (100 PeV). The CASA detector (*C*hicago *A*ir *S*hower *A*rray) [7] of the University of Chicago has been designed and built for UHE cosmic gamma detection.

c) As the cosmic ray flux drops exponentially with the energy, the acceptances, in terms of surface and solid angle coverage must be massively increased to insure acceptable event rates in the EHE (*E*xtrem *H*igh *E*nergy, $E > 10^{17}$ $eV, 100$ PeV) range. Neither Cerenkov, nor charged particle detection at ground level provide the possibility to reach the required acceptances. Fortunately, the large amount of energy

deposited in the atmosphere makes another effect detectable. At such an energy level ($>$ 100 PeV) the fluorescence signal produced by the air molecules desexcitation, mainly N_2 molecules and N_2^+ ions, is large enough to be discriminated against the night sky background. The Fly's Eye detector [8], built following this detection principle, is made of 67 mirrors of 157 cm in diameter. Each mirror is equipped in its focal plane with a set of photomultipliers (PM) with multiple orientations. The telescope has an effective solid angle coverage of nearly 2π steradians. The surface coverage of the system (67 telescopes) depends on the cosmic ray energy and reaches $\sim$ 1000 km^2 at E = 100 PeV.

2.2 Setup used for the simulation

In the simulation the parent particle direction will be determined by Cerenkov imaging. Cerenkov photons collected by the mirror form an image of the emitting particles spatial distribution on the mirror focal plane. The image is recorded by a set of photomultipliers, distributed over that plane. The shower image has roughly an elliptical shape and the ellipse main axis lies in the plane defined by the shower axis and the mirror center as illustrated on figure 1.

Using sterescopic views from two or more telescopes one can reconstruct completely the shower direction. The determination of the ellipse axis direction on each of the images defines a plane containing the shower. The intersection of the two or more planes so defined determines the shower axis.

As discussed in section 5, the availability of more than two observation stations enhance the precision of energy and direction estimation as well as the detector acceptance.

The simulations have been carried out for a configuration of four spherical mirrors, 10 meters in diameter (78.5 m^2) and with a focal length of F = 6 m. Three mirrors are placed such that their centers are 120 meters apart, in an equilateral triangle pattern. The fourth mirror is placed in the center of the triangle. The mirror positions are shown in figure 3.a. The "Standard" equipment of the focal plane consist of:

(i) 91 photomultipliers (PM) of 1" diameter covering the central region. They are arranged in five concentric shells surrounding the central PM. Each shell has 6n (n =1,2,...,5) PM'S in addition to a central PM (n=0), each PM covering 0.25°. These 91 PM'S have thus an angular coverage of $\pm$ 1.375° around the mirror axis.

(ii) 18 2" PM'S, arranged in an external ring around the central region, extend the angular coverage to $\pm$ 1.875°, with a granularity of 0.5° the amplifying camera "standard" configuration is shown in figure 3.b.

The mirror dimensions, and the standard PM configuration have been chosen to be very similar to those used by the Whipple Laboratory in their Mount Hopkins experiment [9] [10] with a single mirror. In the simulation, the data from any mirror combination can be used. In addition the acceptance and the granularity of the focal plane detectors have been varied to study their effect on shower reconstruction. Simulation results with this setup are described in sections 5 and 6.

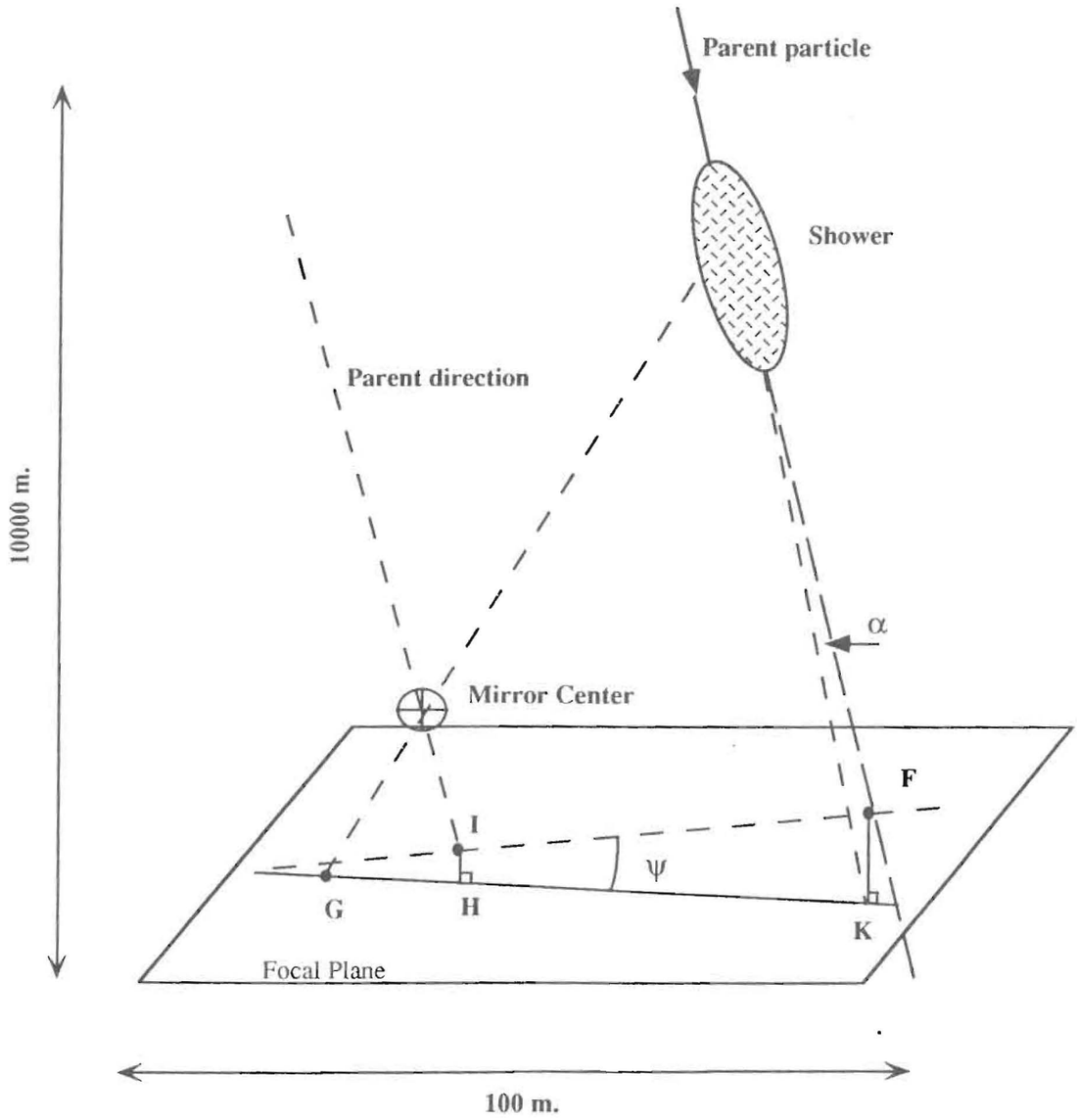

Fig 1 : Shower-Mirror configuration

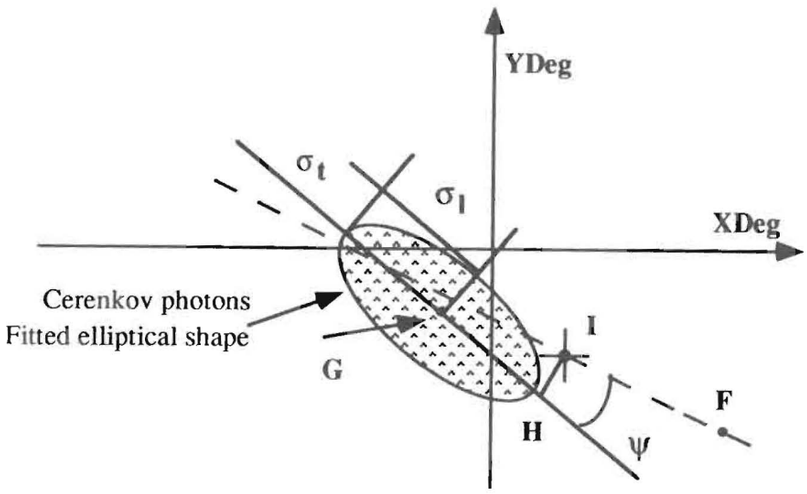

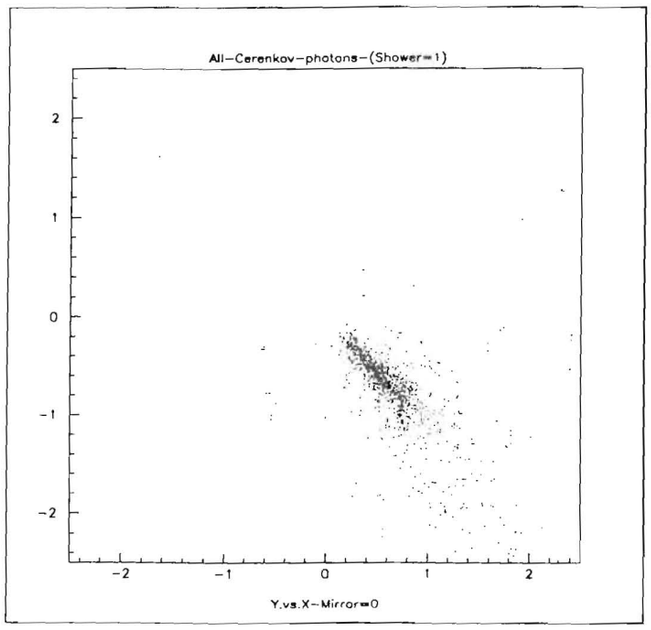

Fig 2 : Shower's image in the focal plane
(a) schematic view and notations.
(b) Example of Cerenkov photon distribution

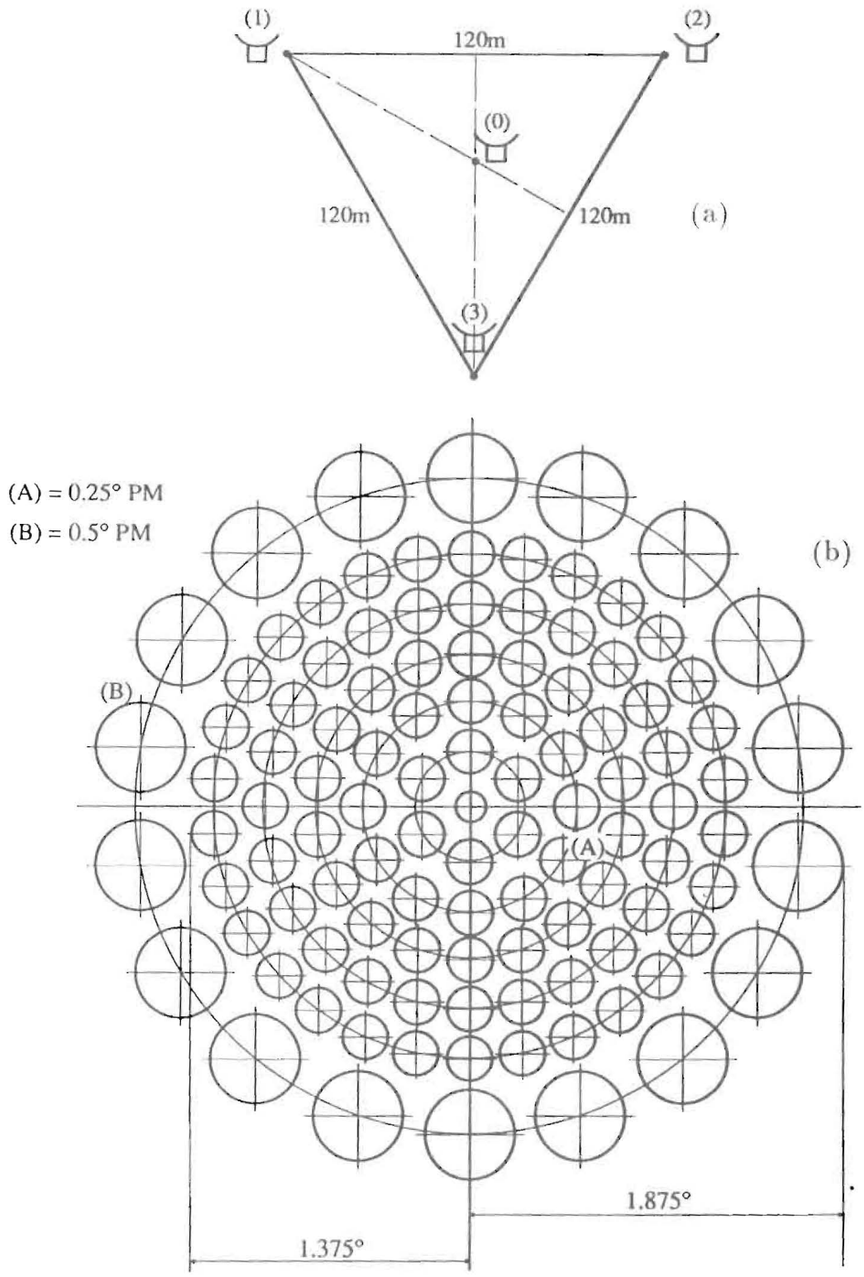

Fig 3 : Detector configuration for simulations
(a) Telescope positions.
(b) Focal plane photomultiplier (PM) equipment.

3 MOCCA. THE ATMOSPHERIC SHOWER MONTE-CARLO GENERATOR

The event generator, developped by A.M. Hillas [11] [12] has been used for the present study. It has been specifically designed for simulation of showers, initiated by cosmic ray particles incident in the earth atmosphere, using pure Monte Carlo Technics. Atmospheric cascades, initiated by protons, nuclei (He^{++}, Li^{+++},...), photons or electrons in the energy range GeV to PeV can be generated. The program is written in Pascal, and the use of recursive programming, available with Pascal has yielded a highly efficient and compact code.

The various physical processes, describing the interaction of high energy particles with matter, which are included in the program are presented in this section (see for example reference [4] for a detailed discussion).

Electromagnetic processes, describing the behaviour of electrons and photons are well understood. Detailed theoretical description, as well as precise experimental measurements are available for these processes. As a result, (see section 3.1) the simulation of electron photon interactions is largely based on precise theoretical calculations. Unfortunately, our knowledge of nuclear interactions has not reached the same degree of maturity and involves more complex phenomena. A phenomenological description of nuclear interactions, shortly presented in section 3.2 below, is used for the simulation of proton and pion behaviour. The thin sampling technique, described below in section 3.3, make it possible to simulate very high energy cascades, up to PeV energy particles within reasonable computing time.

3.1 Electron-Photon cascades

Electrons (e^-) and positrons (e^+), and also other charged particles interact with matter via the following processes:

- Bremsstrahlung
- Ionisation energy losses
- Single and multiple coulomb scattering

In addition, positrons can suffer annihilation through collision with atomic electrons. In the case of atmospheric showers, charged particles are deflected by the earth magnetic field.

Energetic photons can be emitted by charged particles in the strong electric field of the nucleus (Bremsstrahlung). This process is described according to the formulae in reference [6]. The bremsstrahlung rate diverges for low photon energies. This infrared divergence is eliminated by imposing a low energy cut-off on the emitted photon. An energy loss term, corresponding to these low energy photon emission is added to the ionisation energy loss.

Charged particles loose energy through interaction with atomic electrons during their passage through matter. This process produces electron-ion pairs, and occasionnaly a high energy electron, (δ-rav). The production of δ-rays with an energy larger than 1 MeV is implemented in the program as individual collision processes. The ionisation energy loss term describes energy transfers of less than 1 MeV.

Electron and positrons are deflected by the nucleus electric field. This coulomb deflection is treated in a very complete way in the program, to include single, plural and multiple scattering. The annihilation process for positron ($e^+ + e_{(atom)} \rightarrow 2\gamma$) is also included. The curvature due to the earth magnetic field on the charged particle trajectories is taken into account.

Three electromagnetic processes, involving a primary photon can take place in matter:

- Pair creation
- Compton scattering
- Photoelectric effect

In the nucleus field, a photon with sufficient energy ($E\gamma > (2m_e = 1022\ KeV)$) can produce an e^+e^- pair ($\gamma \rightarrow e^+e^-$ in a nucleus field). The compton diffusion ($\gamma + e^-_{Atome} \rightarrow \gamma' + e^-$) ejects an electron from the atom, accompanied by a scattered photon (γ'). These two effects are implemented in the simulation code following the formulae of reference [6].

The photoelectric process, consisting in the absorption of an incoming photon by an atomic electron ($\gamma + e^-_{Atome} \rightarrow e^-$) is included in a more approximate way in the program. The direction of emission of the photoelectron is not accurate. Also simple parameters, instead of detailed tables are used for heavier elements.

Energetic photons ($E\gamma > 100\ MeV$) can also interact inelastically with the atomic nucleus. Photopion production cross-sections are tabulated, and the collision process itself is treated phenomenologically. For photon energies less than few hundred MeV, an intermediate mass baryon, called fireball is formed, which decays into a nucleon (proton) and one or two pions ($\gamma + p/n \rightarrow B^* \rightarrow p/n + \pi_s$). For higher energy photons, the collision is treated as a pion-nucleus collision (see below). Photonuclear resonnances are not included.

3.2 Nuclear interactions

Hadrons (proton, antiproton, pions, ...) interact mainly via strong and nuclear processes although charged hadrons have also electromagnetic interactions. Given the difficulties of theoretical modeling of strong interactions (QCD), the Monte Carlo simulation of hadron behaviour is generally based on phenomenological descriptions.

The collision of a high energy proton with an air nucleus (${}^{7}_{11}N$, ${}^{8}_{16}O$, ...) can be described as the inelastic collision of the incoming proton with an individual nucleon, in the presence of spectator nucleons. Pions ($\pi^0, \pi^{\pm}$) are the main products of that

inelastic process. Collision products (pions and the two nucleons) have a flat rapidity[1] distribution; in the center of mass reference frame (i.e, they are concentrated in the forward/backward cones). The figure below shows schematically the collision process.

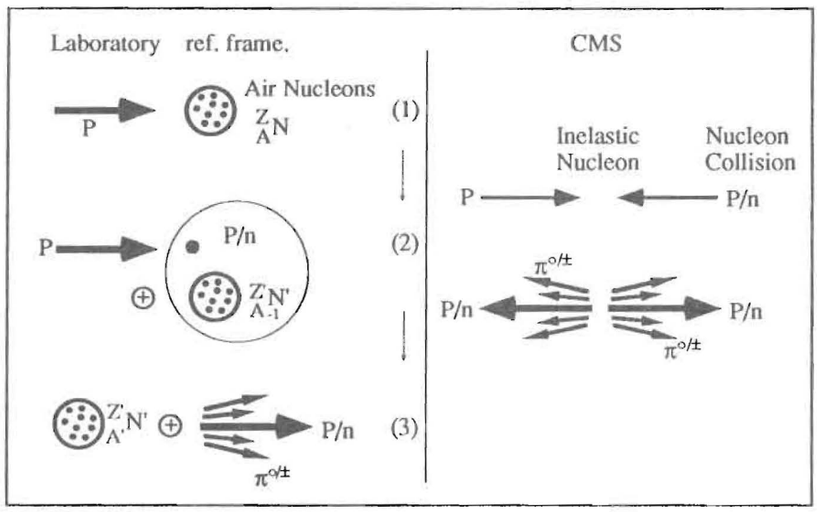

When observed in the laboratory (Earth atmosphere) reference frame, a number of energetic pions, associated with the leading nucleon leave the collision point. The remaining nucleus (an unstable one), as well as other interaction debris carry a small momentum and have thus a negligible effect on the subsequent shower developement. Strange particles (K's) and antiprotons are produced at lower rates in the interaction. Their production processes are not included in the version of the Monte Carlo program used.

The pion spectrum is described phenomenologically by using a scaling law ($x = E_{secondary}/E_{primary}$). The secondary particle spectrum (differential cross-section shape) is thus defined without an explicit energy dependance. A fit to the experimental data, as a function of $x = E_{sec}/E_{prim}$ for the pions spectrum is shown in figure 4 [11]. The angular distribution of emitted pions is determined according to the "Flat Rapidity distribution", which expressed in mathematical terms, gives the following probability distribution for the pions transverse momentum:

$$h(P_t).dP_t = C.P_t\ e^{-P_t/P_0}\ dP_t$$

At first sight, it may seem that a direct method for Monte Carlo generation of the energy spectrum would be to draw randomly distributed values for $x = E_{sec}/E_{prim}$, according to the dn/dx spectrum. But imposing the energy conservation constraint ($\sum_i x_i = 1 \Leftrightarrow \Sigma E_\pi + E_{Leading} = E_{initial}$) would generally produce a distorted spectrum.

[1] Rapidity ξ is defined as: $\xi = 1/2\ Ln\left(\frac{E+P_{//}}{E-P_{//}}\right)$, $P_{//}$ being the component of the momentum along the colliding system trust axis. For $E \gg mc^2$, $\xi \simeq -Ln(tg(\theta/2))$. θ is the particle angle in respect to the trust axis.

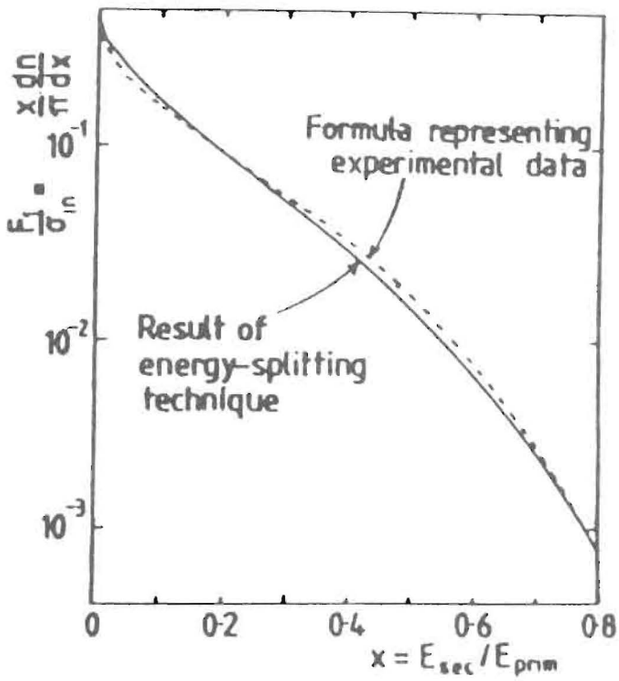

Fig 4 : x = $E_{sec}/E_{primary}$ spectrum in nuclear interactions

In the energy splitting method, developed by A.M. Hillas the emission process is modelled as successive two body decays of the excited system. The radiated energy A_0 (A_0 = kinetic energy of the incoming proton) is divided randomly in two parts A_1, B_1 ($A_0 = A_1 + B_1$). This splitting process is repeated for each available energy part:

$$A_i = A_{i+1} + B_{i+1} \text{ if } A_i \text{ not emitted as } \pi^{o/\pm}$$

$$B_i = A'_{i+1} + B'_{i+1}$$

At each stage, the energy part A'_i can be either emitted as a pion of total energy A'_i, or else is made available for further splitting. The process is repeated until the available energy packets are smaller than pion masses. The splitting rules, determining whether an energy packet is emitted as a particle or split further, differ for nucleon and pion primaries. A detailed description of these empirical rules can be found in [11]. The x spectrum obtained by this method is also shown in figure 4 (full curve) and agrees well with the fit to the experimental data (dashed curve).

In the case of an atomic nucleus primary, the collision with an air nucleus is modeled as the superposition of one or more inelastic nucleon-nucleon collisions, accompanied by elastically freed nucleons, α-particles and usually a remaining nucleus, from the incident cosmic ray particle. The primary particle kinetic energy is divided evenly among the nucleons. The elastically freed particles have thus a large momentum relative to the earth atmosphere. They are followed by the simulation program along with the secondary energetic particles from the inelastic collisions.

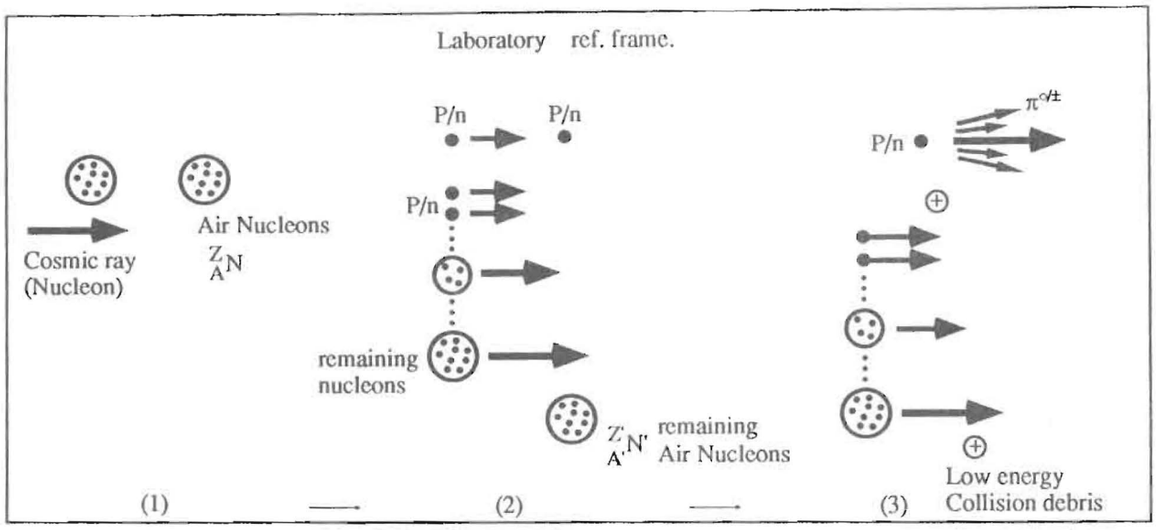

3.3 Thin sampling

An important technical feature of the Monte Carlo program is the "Thin Sampling" which makes possible the simulation of very high energy showers by pure Monte Carlo method. The thin sampling consists of following only a fraction of low energy secondaries. A demarcation energy E_{th} is chosen, typically $\simeq 10^{-4}\ E_{primary}$. All particles with energy $E > E_{th}$ are followed, while low energy particles $E < E_{th}$ are subject to a selection test.

Such secondaries ($E < E_{th}$) are retained with a probability $p = E/E_{th}$, and assigned a weight $w = 1/p (w > 1)$ when retained. When a particle with weight $w > 1$ interacts, the daughter particles, when retained are assigned a weight $w' = w_{parent} \times 1/p'$ ($p' = E'/E_{th}$). The method is implemented in a way such that the weighted energy ($\Sigma w.E$) is exactly conserved. The selection test is independant of particle type, direction or position. Another important point is the fact that particles produced in different generation of a cascade are treated in an identical way.

When the thin sampling procedure is applied, the number of particles followed during shower simulation is related logarithmically, instead of linearily, to the incident particle energy. The method is discussed in reference [11]. This economical technique provides the possibility of VHE cascade simulation.

3.4 Cerenkov photons

Although Cerenkov light plays a crucial role in the shower detection and measurement, the energy lost by this mechanism is extremely small, and Cerenkov photons have no effect on the cascade process. For this reason, the Cerenkov radiation is not treated as a standard shower developement process such as bremsstrahlung or Coulomb scattering. Rather, it is implemented as a detector simulation set.

For all charged track segments, the amount of light collected by the mirrors is

computed using the Cerenkov emission angle. Also, for each track segment, the total number of emitted Cerenkov photons, in the light detector (PM) sensitivity wave band is calculated taking into account the atmospheric transmission. The mean number of Cerenkov photons, originating from the charged track segment, and reaching the mirror is then determined. The actual number of photons reaching the mirror is generated according to the Poisson law. The photons are distributed randomly over the Cerenkov cone. Their impact point on the mirror, and their directions are recorded for further processing. The air refraction index is derived from the density:

$$n = 1.0 + 0.0002977.\ \text{Density}/0.129$$

Density expressed in Gram/cm^3

Air density as a function of the altitude is calculated using a multilayer atmospheric model. This is shown on figure 5.a. The corresponding refraction index and the Cerenkov emission angle (mrad) are represented on figure 5.b and 5.c ($\theta_{Cerenkov} = Arc\ Cos(1/\beta n)$). The atmospheric transmission for an observation site at z = 0 m (z = 2300 m), as a function of emission altitude is shown on figure 6a (6b), at zero degree viewing angle. The transmission at 45° viewing angle, and at a 2300 m observation altitude (Whipple observatory altitude) is shown on figure 6c.

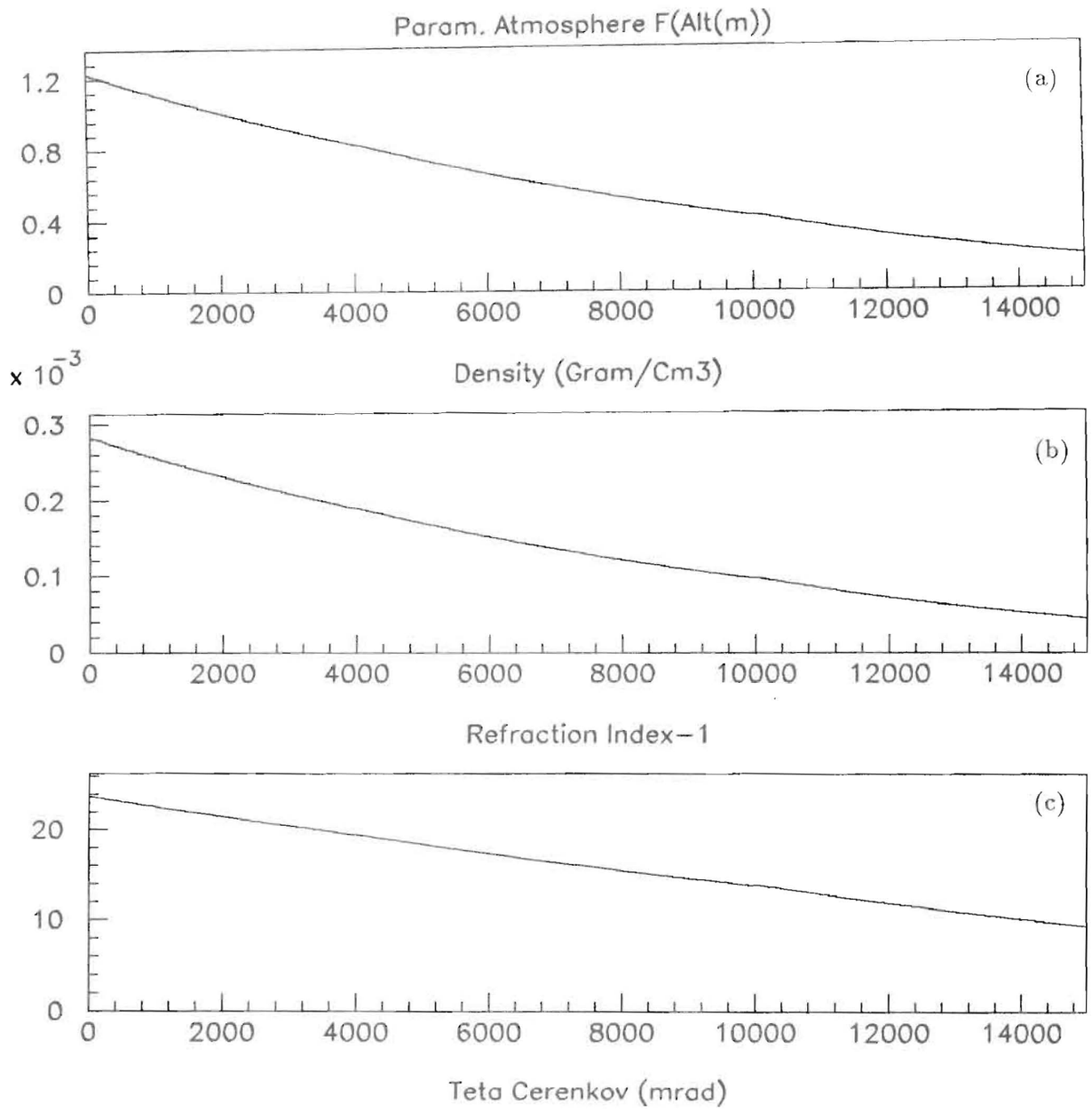

Fig 5 : The multilayer atmospheric model
(a) Density (Gram/cm^3) = F (Altitude)
(b) n-1 = F (Altitude) n= Refraction index
(c) $\theta_{Cerenkov}$ (mrad) = F (Altitude)

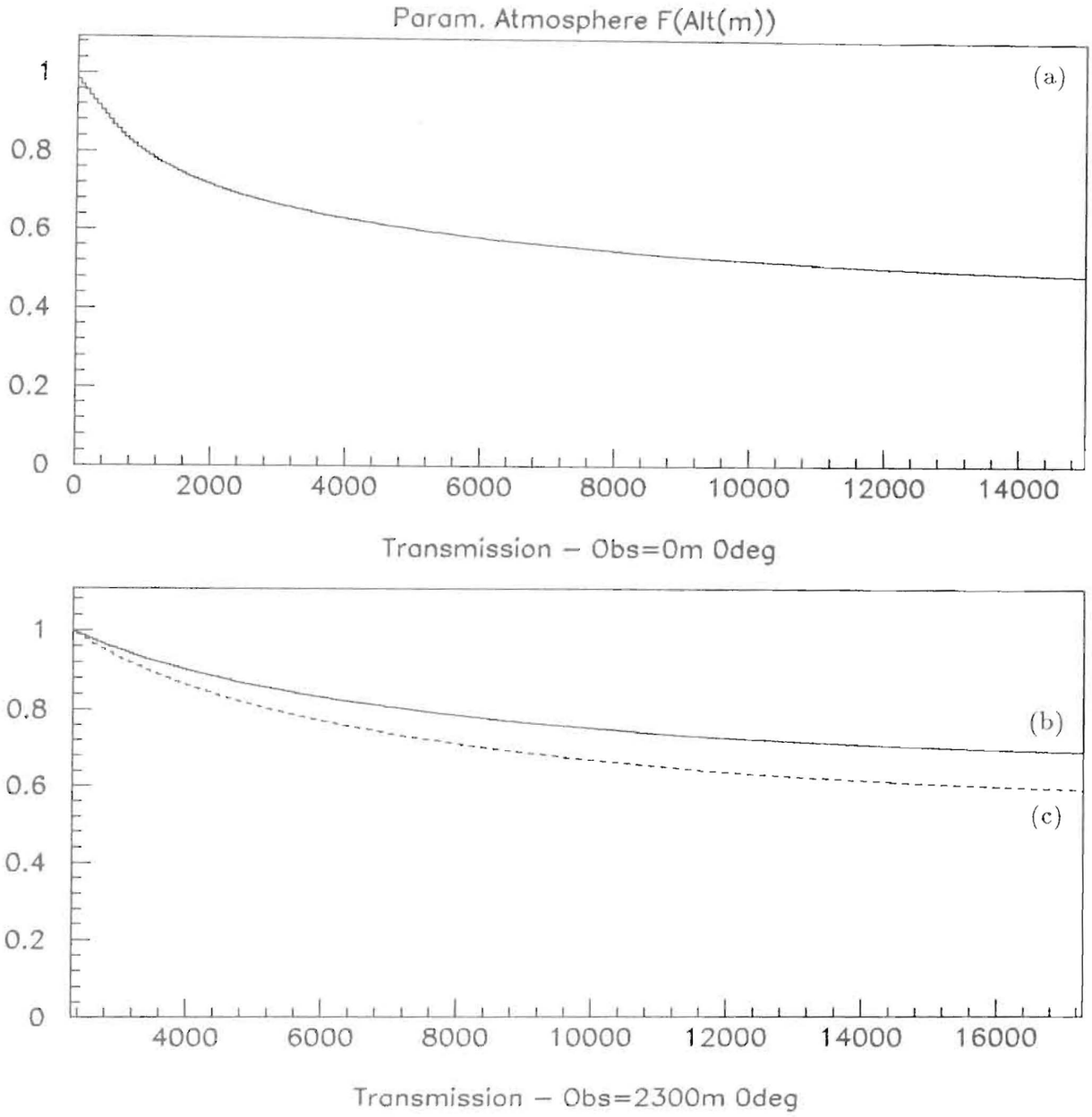

Fig. 6 : Atmospheric transmission in the visible range, zero degree viewing angle observation at sea level (a), at 2300 m (b) : F (Altitude)
(c) 45° viewing angle, Observation at 2300 m

4 SHOWER GENERAL CHARACTERISTICS

In this section, we discuss extensive air shower properties, especially from the Cerenkov detection point of view. As much as possible, we have tried to keep the results presented in this part independent of a specific experimental setup. They are based on the study of showers generated with a fixed direction and ground impact point. The Cerenkov photons are collected by a set of mirrors located at various distances from the cosmic ray ground impact point (GIP).

Nucleon showers are generated at zero degree zenith angle for three different primary energies, 1 TeV, 2 TeV and 4 TeV. A comparison with 1 TeV photon initiated showers is also included. The effect of the increased atmospheric depth and light absorption for inclined showers is illustrated by the results for 4 TeV proton showers, at 45° zenith angle.

The characteristics of the event samples used for this study are summarized in Table 1. The mean CPU time spent for one event generation in each case is also indicated. The event generation and analysis has been carried on the IBM 3090-600 E mainframe at IN2P3 computing facility.

Event Sample	Nb. Of Showers	CPU Time/shower
1 TeV proton showers - 0° zenith angle	126	30 sec.
2 TeV proton showers - 0° zenith angle	83	45 sec.
4 TeV proton showers - 0° zenith angle	143	60 sec.
4 TeV proton showers - 45° zenith angle	186	60 sec.
1 TeV gamma showers - 0° zenith angle	159	60 sec.

Table 1: Event samples (CPU Time in IBM 3090-600E Seconds)

4.1 Global shower picture

In order to give the unfamiliar reader a synthetic representation of extensive air showers, we have included bidimensional images of a few showers.

Figure 7, 8 and 9 represent three 1 TeV proton showers, at zero degree zenith angle. The successive positions of all particles with an energy larger than 25 MeV in the X-Z plane are plotted. The intervals between the dots correspond to the lengths of the track segments (muons or high energy particles). The energy cut corresponds approximately to the Cerenkov energy threshold for electrons at sea level [2].

In part (a) of each figure (7.a, 8.a, 9.a), the complete shower is shown by tracing all particles (proton, $\pi^0, \pi^{+/-}, \mu^{+/-}, e^{+/-}, \gamma$) with energies above 25 MeV. The hadronic skeleton of the showers is represented (proton, $\pi^{+/-}$) in figure 10.b and 11.b.

[2] $\theta_c = \arccos((1/\beta n)$; threshold velocity $\beta_t = 1/n$, $n_{air} \simeq 1.000293 \rightarrow [\beta_t]_{air} \simeq 0.999707$, $\gamma_t = 1/\sqrt{1-\beta_t^2} \simeq 42$. $[E_t]_{electron} = \gamma_t\, m\, c^2 \simeq 21.5 MeV$.

The muon tracks are plotted in part (c) of the figures (7.c, 8.c, 9.c). An identical energy cut ((E > 25 MeV) has been applied for the hadronic skeleton and muon tracks representation.

Electromagnetic showers, as expected, have a much more regular shape. This is illustrated by the figure 10, where three 0.5 TeV photon initiated showers are shown. All particles (photons and electrons) with an energy larger than 25 MeV are traced in the X-Z plane on figure 10.a, 10.b and 10.c.

Multiple electromagnetic branches are a common characteristic of hadronic showers, as it can be seen on figure 7-9. Proton showers are thus spatially more extended than photon showers which have a dense and well defined core. To provide more quantitative information on this point , the lateral shower profile and the particles angular distribution have been computed. The particle distribution for the shower of figure 7 (1 TeV proton shower) at three altitudes, namely 14000 m, 10000 m and 7000 are shown in figure 11. The X-coordinate distribution for particles above 25 MeV is shown on figure 11.a, and their angular distribution, relative to the primary particle direction on figure 11.b. Figure 12 shows the same distributions for the photon shower of figure 10.a. The photon shower profiles are computed for z = 7000 m, z = 10000 m and z = 12000 m. Note that the vertical scales in figures 11 and 12 are arbitrary and do not corresponds to the real particle densities.

As can be seen on figure 11.b and 12.b, the width of the the secondary angular distribution ($\sim 5^{\circ}$) is large compared to the Cerenkov emission angle in air ($\sim 1^{\circ}$), which explains the rather efficient detection of air showers in Cerenkov detectors.

4.2 Cerenkov photon yields

The number of Cerenkov photons collected is a crucial parameter in the detector design. It depends on various parameters including the mirror area, the photodetector efficiency and the focal plane coverage.

We present below the results of simulations of the Cerenkov photon yields, mainly as a function of the distance separating the mirror center and the primary impact point at the detection level. The results are given as Cerenkov photon densities, i.e the number of $\check{C}$ photons per mirror unit area (1 m^2).

These densities correspond to photons with angles less than 1.4° relative to the mirror axis. The effect of a the focal plane acceptance will be discussed in the next section. The atmospheric light absorption (see section 3.4), the mirror and the light detector (PM) efficiency have been taken into account. The numbers presented here have been obtained assuming a mean light collection efficiency of 12 %, over a waveband of 3.85 10^{14} hz, for the mirror-photodetector system.

To obtain these densities, showers are generated with fixed energy, direction and ground impact point (GIP). Eight (8) mirrors are placed at various distances from the shower impact point (GIP), from 0 up to 190 meters. The observation site altitude corresponds to that of the Mount Hopkins observatory, i.e 2300 meters above sea level.

In addition to the mean Cerenkov densities, the shower to shower fluctuation around the central value is also given by the error bars on the figures.

Figure 13 shows the Cerenkov photon density, as a function of the mirror - GIP

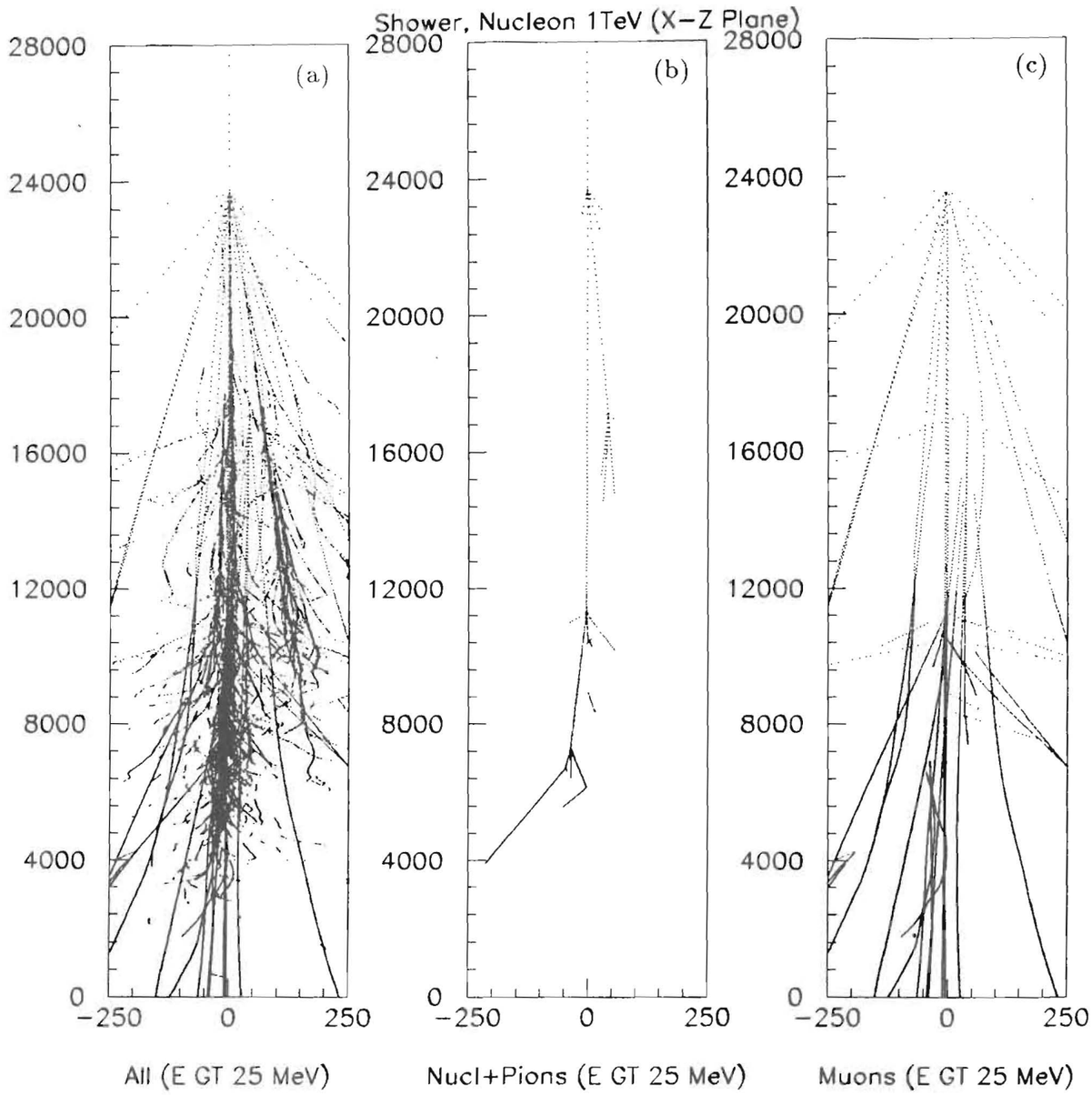

Fig 7 : 1 TeV proton shower, at zero degree
(a) All particles, $E > 25$ MeV
(b) protons $\pi^{+/-}$, $E > 25$ MeV
(c) Muons $E > 25$ MeV

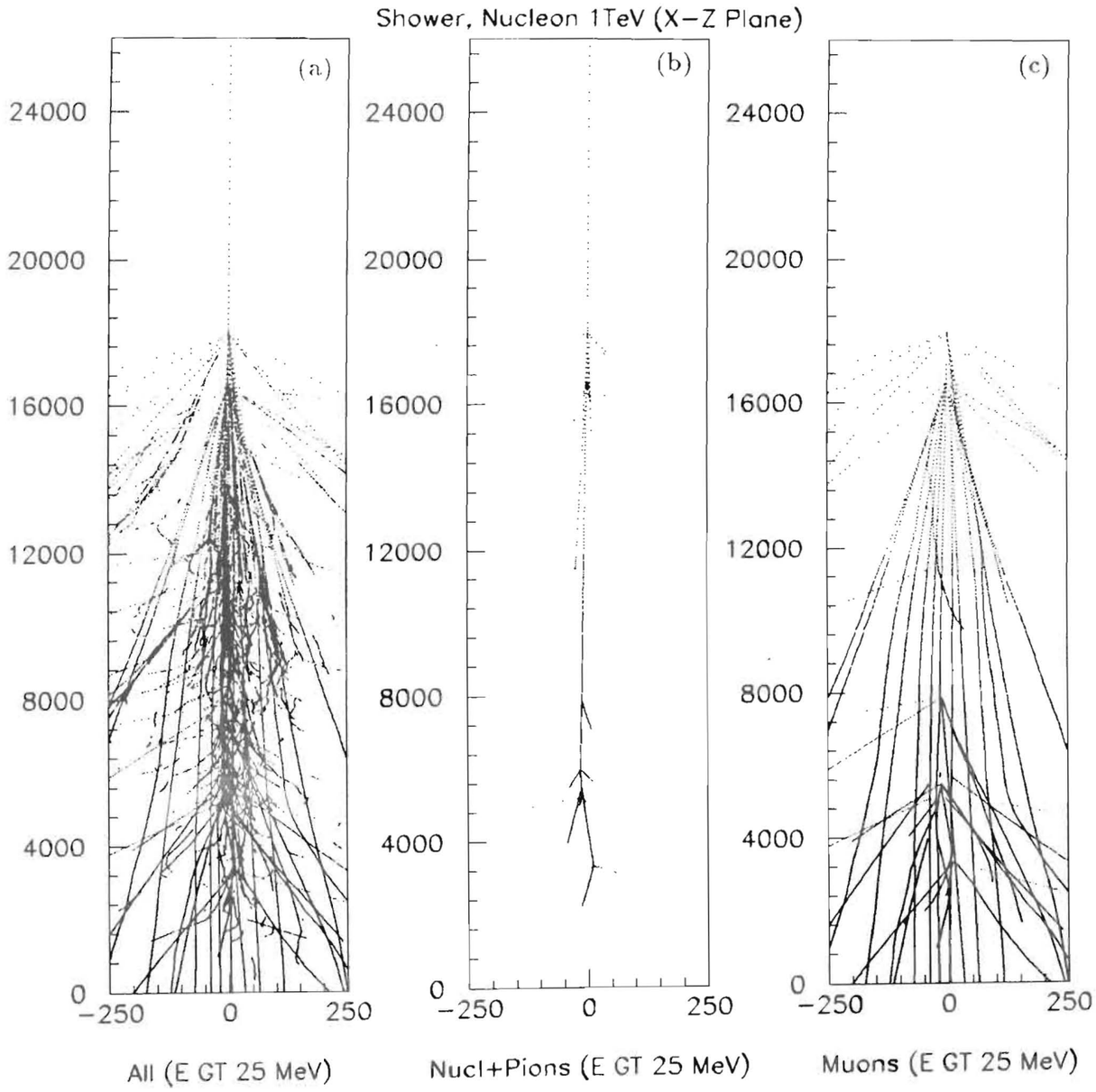

Fig 8 : 1 TeV proton shower, at zero degree
(a) All particles, $E > 25$ MeV
(b) protons $\pi^{+/-}$, $E > 25$ MeV
(c) Muons $E > 25$ MeV

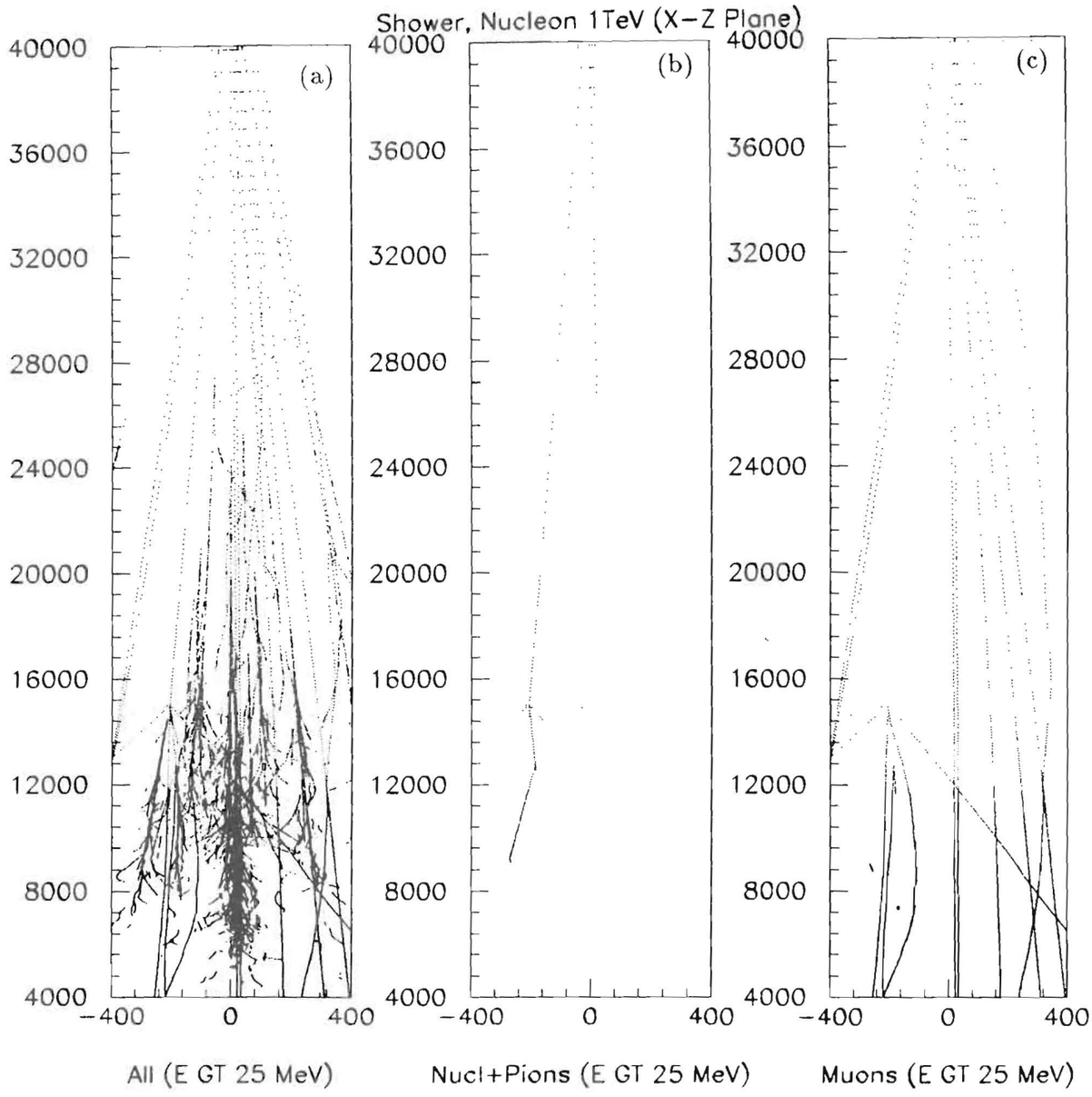

Fig 9 : 1 TeV proton shower, at zero degree
(a) All particles, $E > 25$ MeV
(b) protons $\pi^{+/-}$, $E > 25$ MeV
(c) Muons $E > 25$ MeV

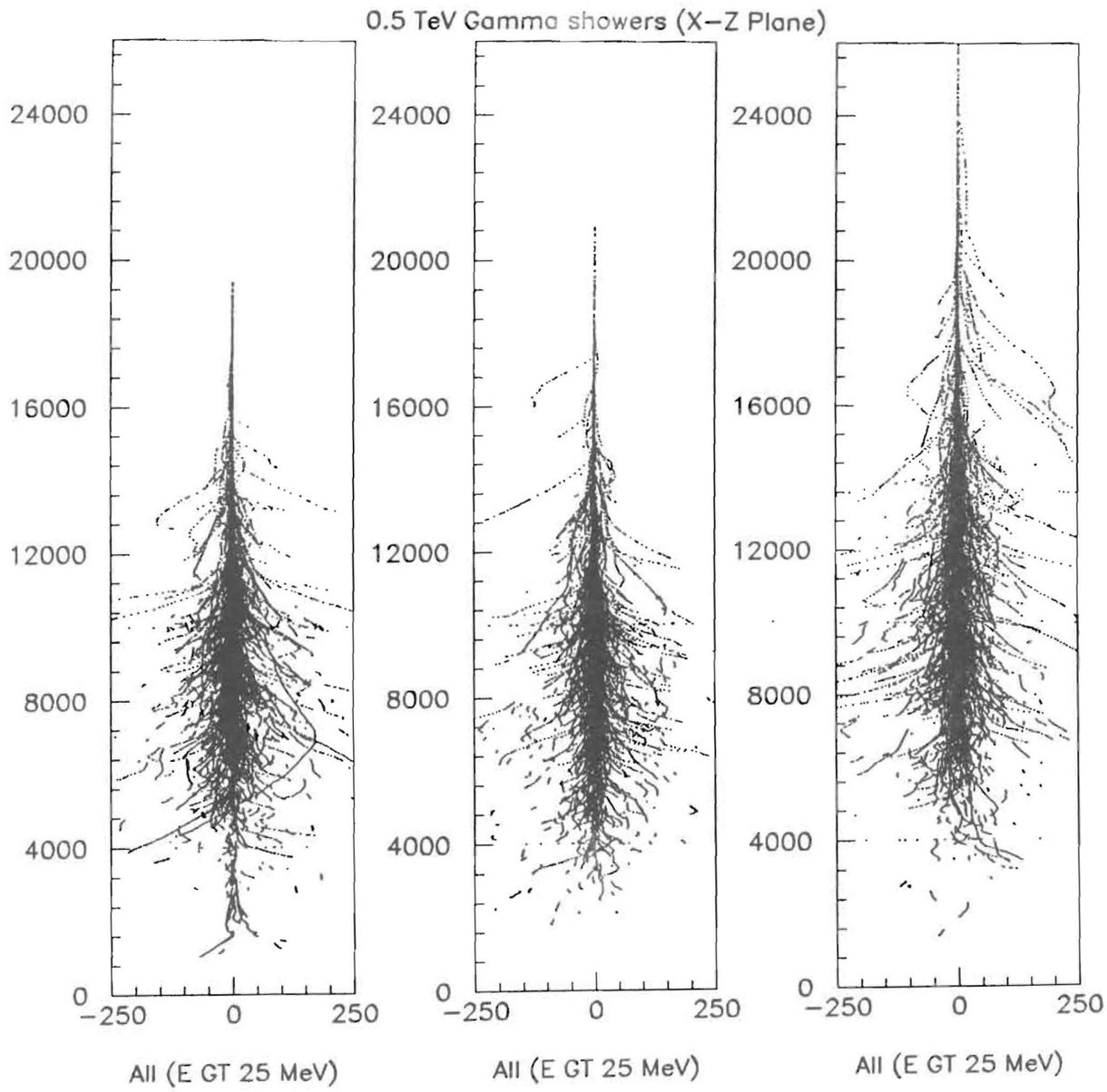

Fig 10 : Three 0.5 TeV Gamma showers (a) (b) (c)

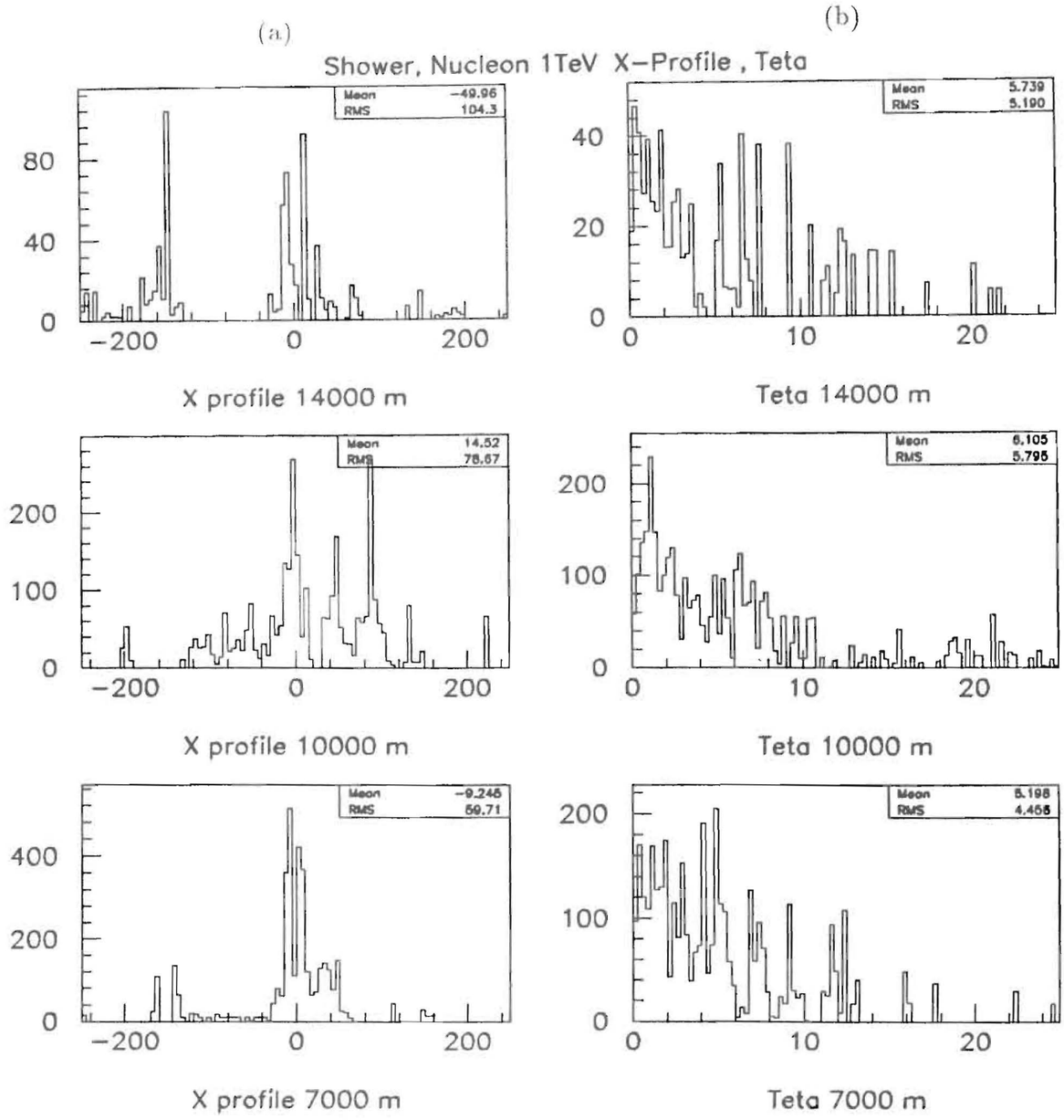

Fig 11 : X-profile (m) and angular distribution (mrad) at Z = 7000 m, 19000 m and 14000 m for a 1 TeV proton shower

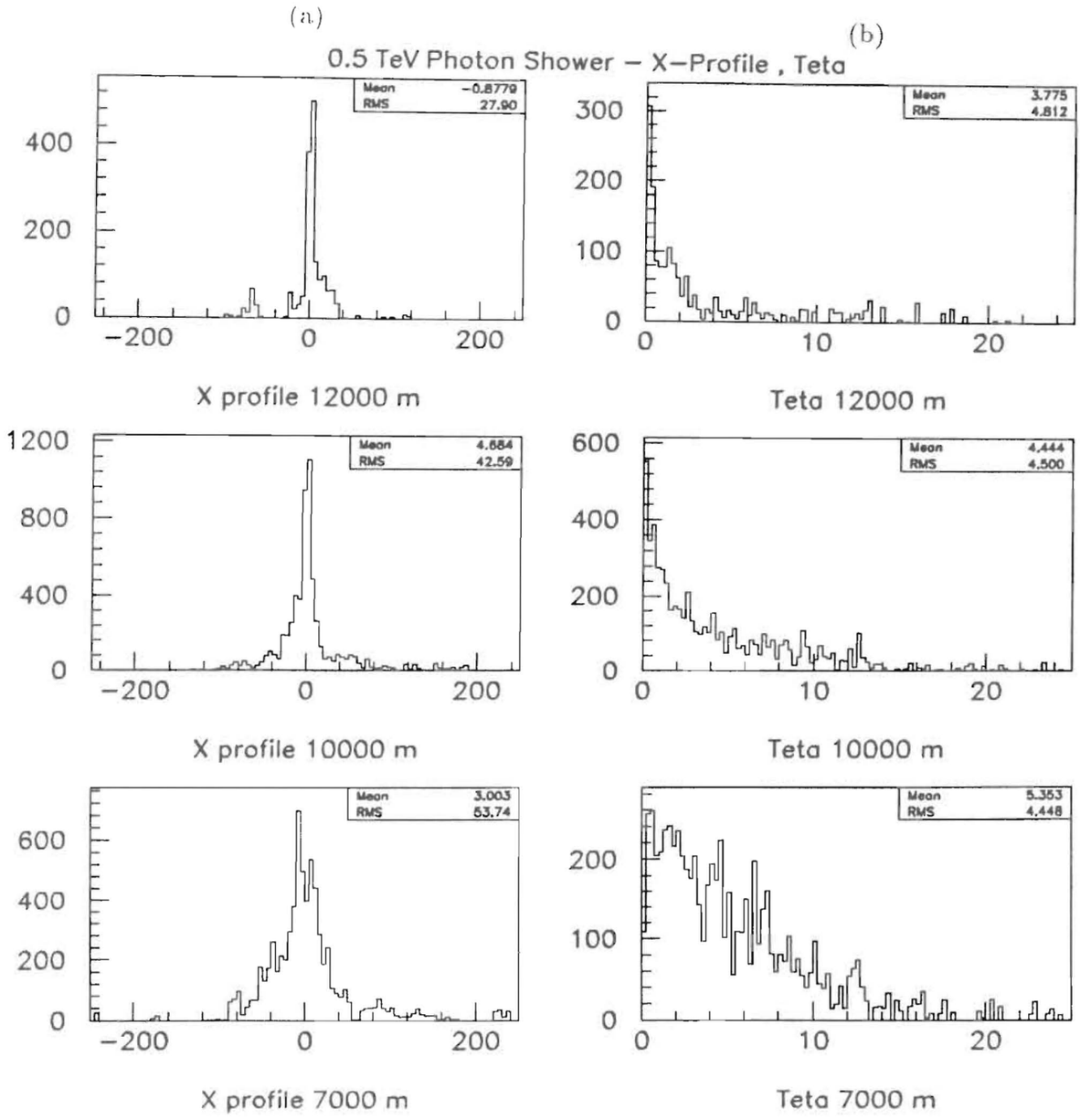

Fig 12 : X-profile (m) and angular distribution (mrad) at Z = 7000 m, 10000 m and 12000 m for a 0.5 TeV Gamma shower

distance for nucleon (proton) initiated showers. The plots of figures 13.a, 13.b, 13.c correspond respectively to 1 TeV, 2 TeV and 4 TeV showers.

Two important features of the nucleon showers are apparent from these three plots:

- The Cerenkov photon density decreases exponentially. The effect is more pronounced at higher energies.
- The Č photon yield increases faster than the primary energy. As the total path of the secondary particles is proportional to the primary energy to a very good approximation, one might expect a scaling behaviour of the Cerenkov densities, contrary to what is obtained.

The two observed characteristics have the same origin. As the primary energy gets higher, the shower development length increases and there are more energetic secondaries which get close to the detection mirrors. Those parts of the shower can only be seen by the mirrors located near enough to the ground impact point, GIP ($\sim 20 - 30$ meters). Their contribution is responsible for the two observed effects.

For a quantitative measurement, a simple exponential function A exp(-B.d_{M-GIP}) has been fitted to the Cerenkov photon density. d_{M-GIP} is the mirror to the GIP distance in meters. The fitted curves as well as the values of the A and B parameters are shown on figure 13.

In a simulation program, photons may be tagged according to the parent particle type. The Cerenkov photon density from muons in 4 TeV proton showers is plotted in figure 14. Their contribution to the total Cerenkov photon number is small, around 10-20 %. However due to the simplified representation of hadronic interactions (cf. section 3), the muon production may be underestimated.

At comparable energies ($\sim TeV$), the Cerenkov light pattern at the ground level is different for gamma showers. Figure 15 shows the Cerenkov density for 1 TeV Gamma showers, the number of collected photons decreases slowly up to 100 meters from the ground impact point. That does reflect the shower shape which consists mainly of a compact and well defined core located at around 10000 meters in altitude.

Inclined showers see an atmospheric thickness larger than vertical showers. Also the light path for Cerenkov photons is larger, leading to an increased absorption. Figure 16 shows the photon yield for 4 TeV proton showers at 45° zenith angle. The mirrors were placed along an axis perpendicular to the primary direction. The increased atmospheric thickness and absorption result in an important reduction of the number of collected Cerenkov photons and in a weaker dependence of the photon density with the mirror-GIP distance. However, due to their very large mean free path, the muons contribution to the total Cerenkov photon number is increased, up to 25 %, as it can be seen in figure 16.b.

4.3 Cerenkov Telescope Acceptance

In the previous section, we have studied the Cerenkov density dependance upon the distance to the primary ground impact point. For a given detection threshold, it is then possible to compute the effective surface coverage of a single or a set of Cerenkov telescopes.

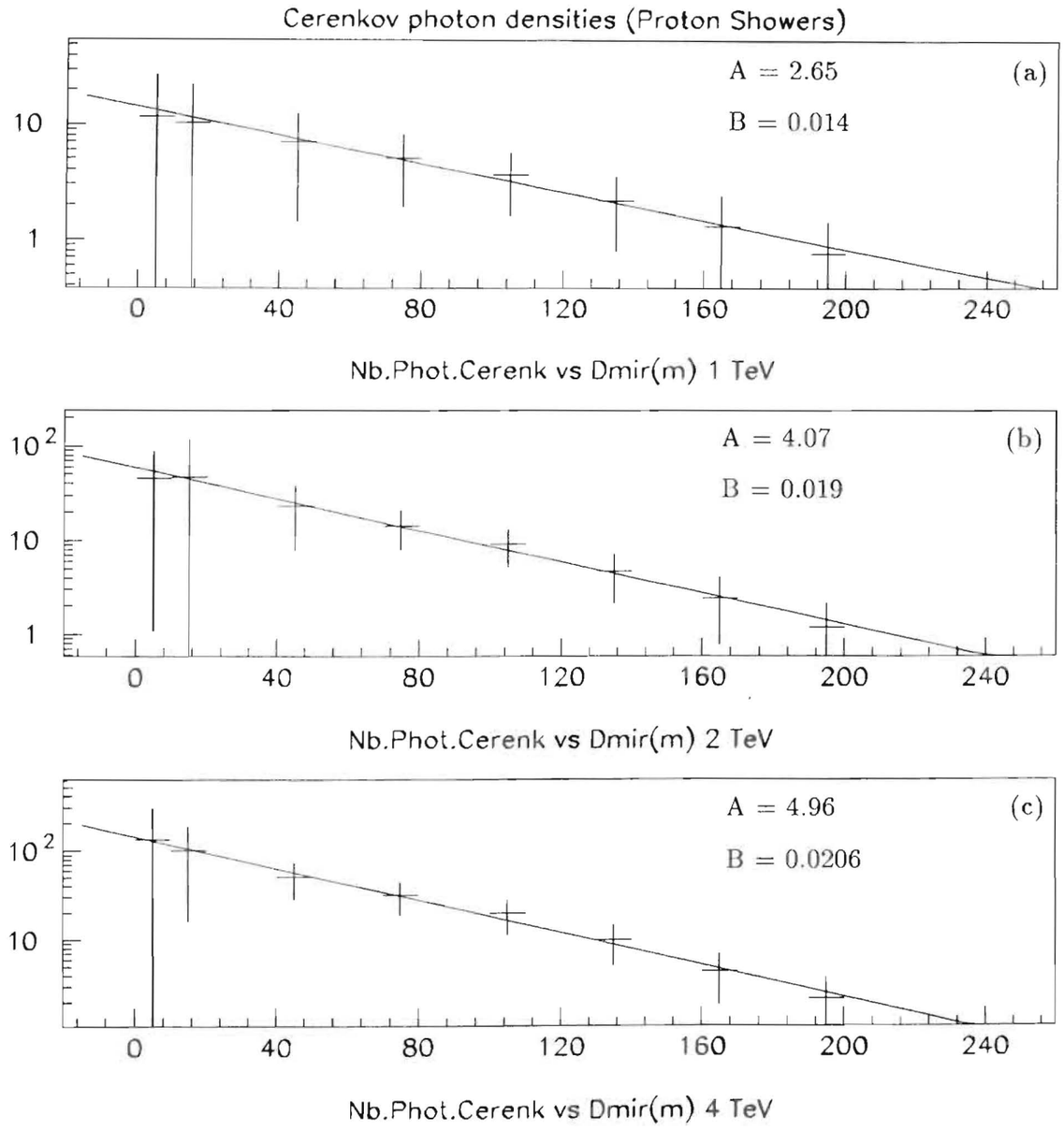

Fig 13 : Cerenkov photon density : F (Mirror-Ground Impact point distance (m))
(a) 1 TeV, (b) 2 TeV, (c) 4 TeV nucleon showers
with fitted exponential Ae^{-Bd} curves

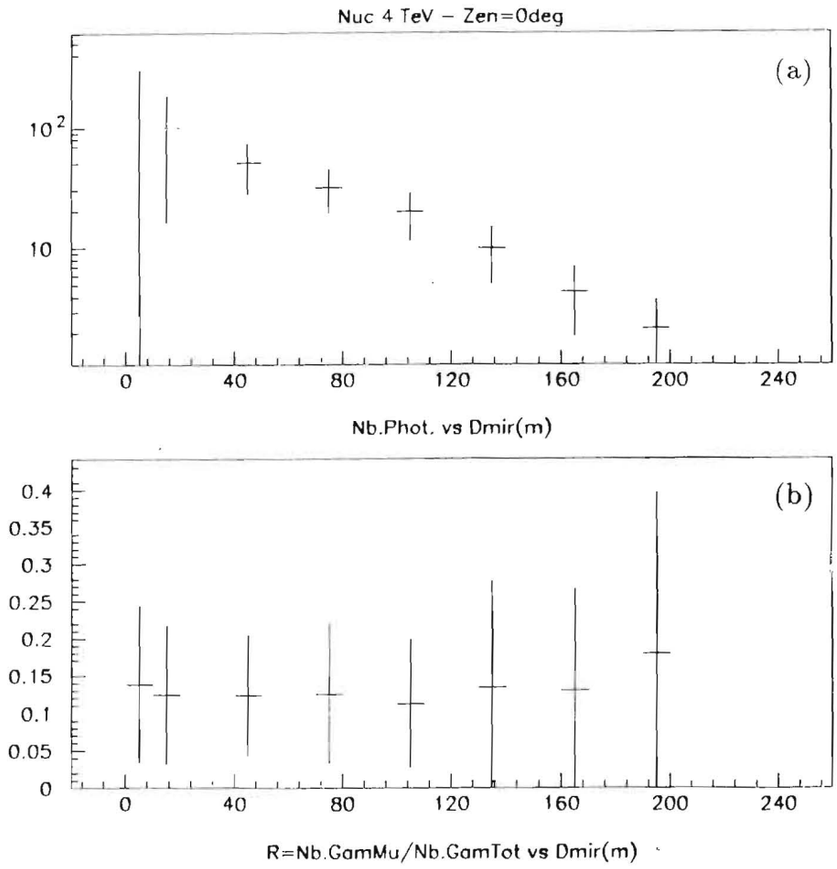

Fig 14 : 1 TeV Nucleon showers, $\check{C}$ photon densities from secondary muons (a) and $R = [N\gamma]\mu \,/\, [N\gamma]tot$ (b) as a function of GIP-Mirror distance

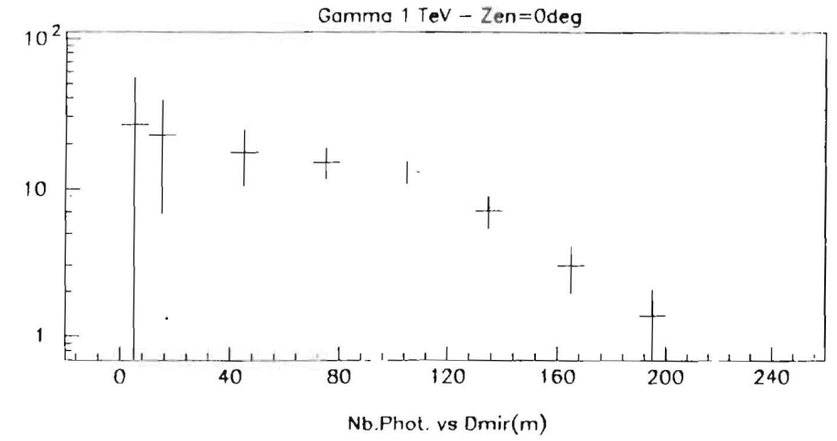

Fig 15 : 1 TeV photon showers, $N\gamma = F(d_{GIP-Mirror})$

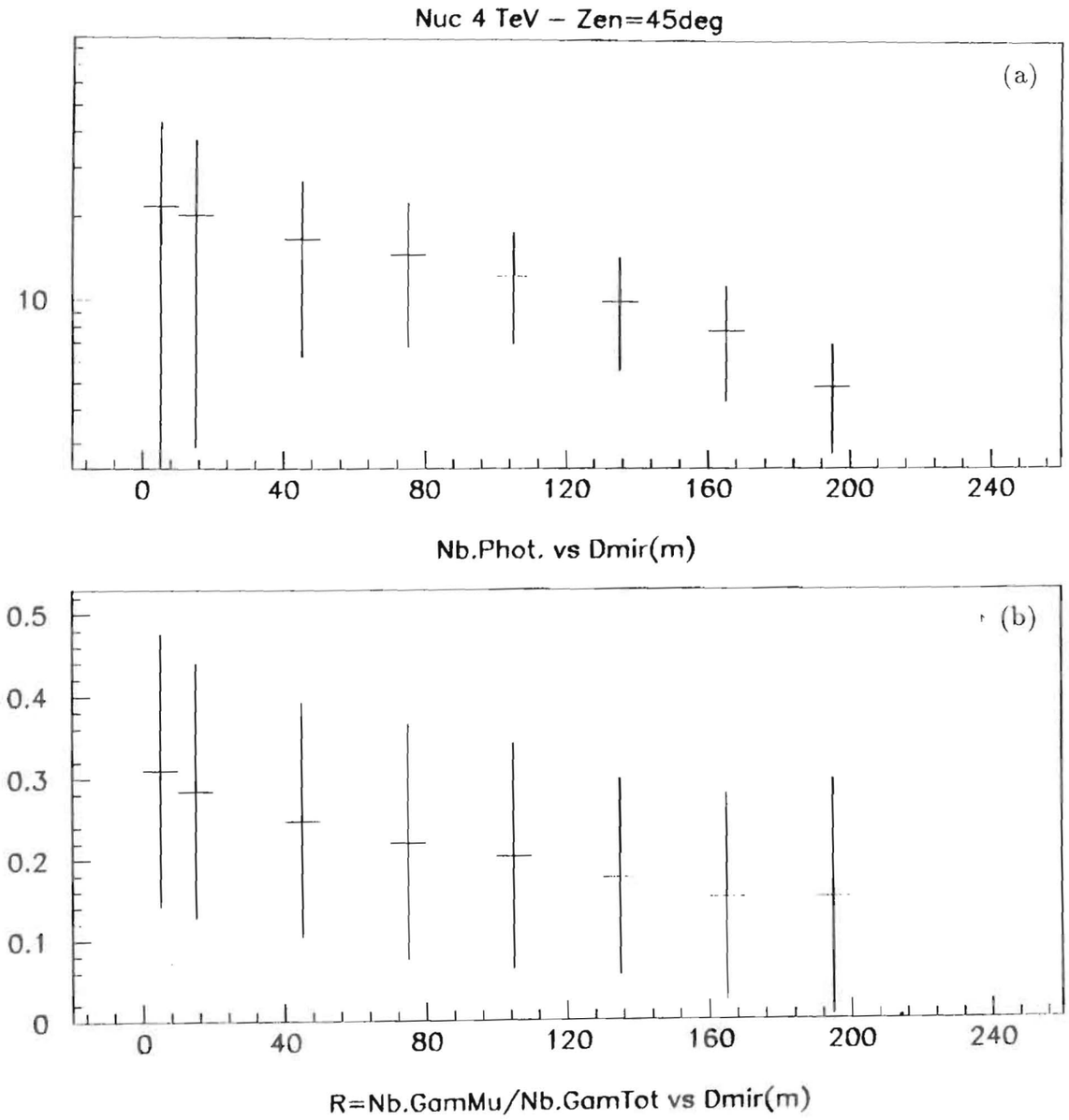

Fig 16 : 4 TeV Nucleon showers at 45°
Total photon yield $N\gamma$ (a) and $R = [N\gamma]\mu$ / $[N\gamma]tot$ (b)

A focal plane coverage over a circle of 1.375° in radius has been assumed in section 4.2. In this section the effect of the focal plane coverage on the number of collected photons will be studied.

The distribution of the angular distance Rdeg $= \sqrt{Xdeg^2 + Ydeg^2}$ (in degree) from the focal plane center, has been computed for the collected Cerenkov photons. The Rdeg distributions for photons produced by 4 TeV proton showers (zero degree zenith angle) and collected at 40 meters and 70 meters of the primary ground impact point (GIP), are shown in figure 17. The same distributions restricted to Cerenkov photons from secondary muons are represented in figure 18. These figures illustrate the rather large focal plane acceptance ($\Delta\theta \simeq \pm 2°$) necessary to collect a significant fraction of the photons reaching the mirror. Similar distributions for 1 TeV Gamma initiated showers, represented on figure 19, show that Cerenkov photons are better collimated in the case of purely electromagnetic shower. The mean Rdeg values for mirrors situated at various distances of the primary impact point are shown on figure 20.b for 4 TeV nucleon showers, and on figure 20.a for 1 TeV Gamma showers.

The effect of the limited focal plane coverage is caracterized by the fraction of the total number of photons reaching the mirror which is effectively detected. Figure 21 shows this collection ratio as a function of the focal plane coverage for 4 TeV proton showers, at 40 meters (Fig. 21.a) and 70 meters (Fig. 21.b) from the GIP. The collection ratio in the case of 1 TeV Gamma initiated showers, is represented in figure 22 under the same conditions.

The number of collected photons as a function of the angular offset between the mirror axis and the primary direction is shown in figure 23 for the case of 4 TeV proton showers (0° zenith angle). As for the focal plane coverage, the photon density is presented for mirrors placed at 40 meters (Fig. 23.a) and 70 meters of the GIP (Fig. 23.b). The horizontal axis represents the mirror axis primary direction offset in degree. The Cerenkov density angular offset dependance for 1 TeV Gamma showers, is shown in figure 24. The figures 23 and 24 correspond to a focal plane coverage of 1.375°. For a 1.5° degree offset, the number of collected photons is decreased by a factor about 2. The effective Cerenkov Telescope solid angle coverage can only be estimated when parameters such as the detection threshold and the focal plane sensitive surface are known. However by considering the factor 2 as an effective detection limit, one obtains a solid angle acceptance $2\pi\ \theta^2/\theta = \pi \times (2.6\ 10^{-2})^2 = 2.15\ 10^{-3}$ steradians.

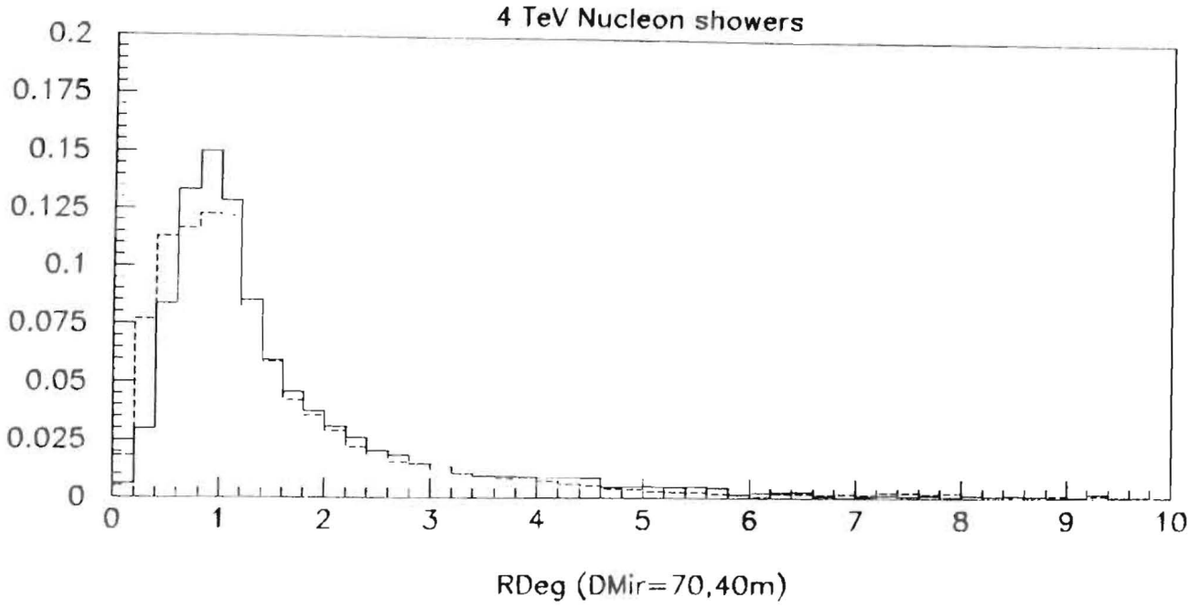

Fig 17 : Rdeg distribution (4 TeV proton showers) for Č photons collected at 40 m (dashed) and 70 m (full) of the GIP

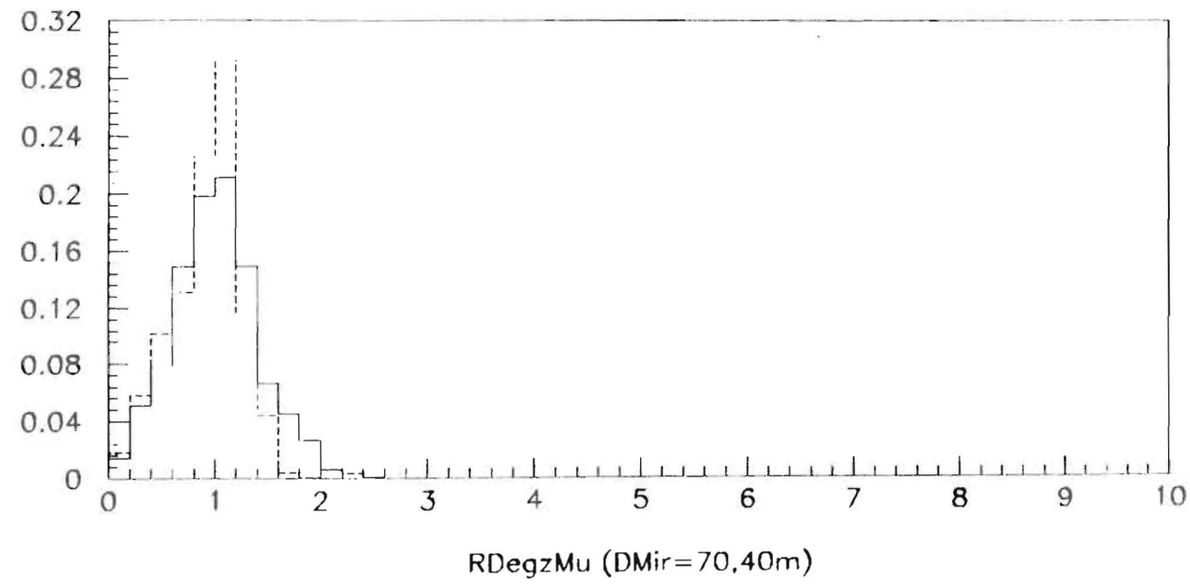

Fig 18 : Rdeg distribution (4 TeV proton showers) for Č photons from μ's collected at 40 m (dashed) and 70 m (full) of the GIP

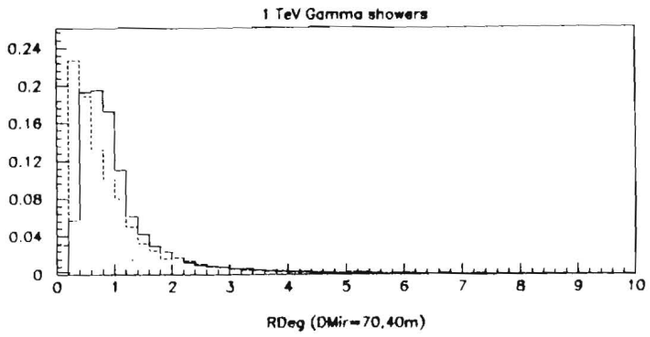

Fig 19 : Rdeg distribution (1 TeV Gamma showers) for Č photons collected at 40 m (dashed) and 70 m (full) of the GIP

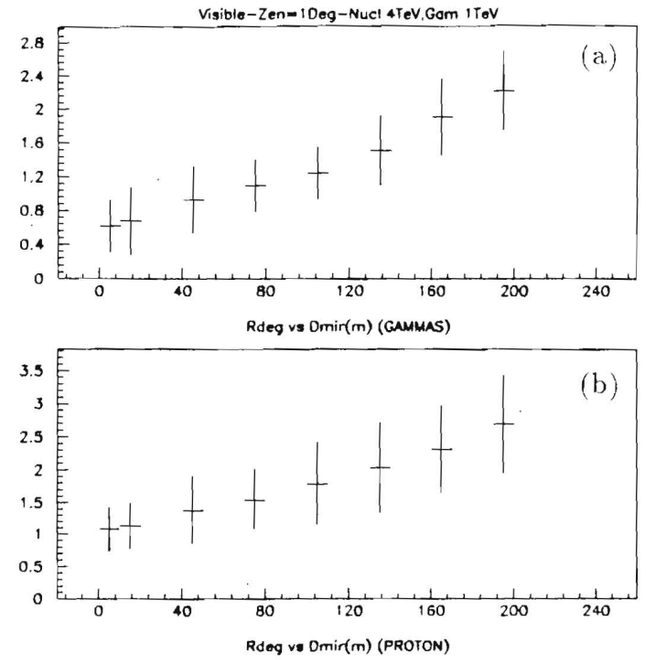

Fig 20 : Mean Rdeg Value $< Rdeg > = F(d_{GIP-Mirror})$
(a) 1 TeV Gamma showers
(b) 4 TeV Nucleon showers

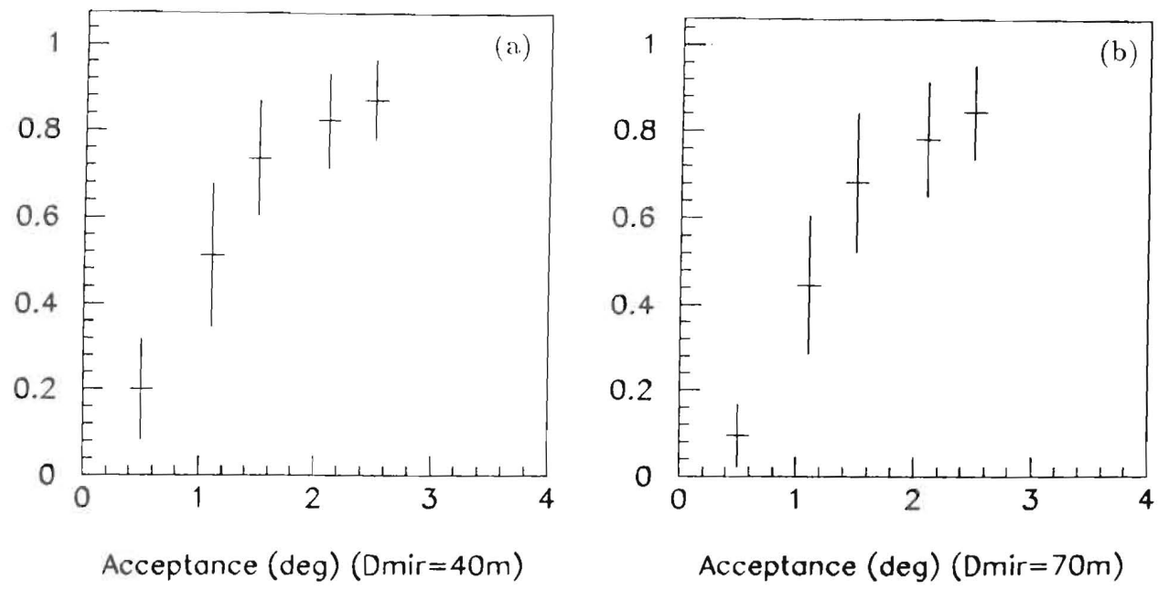

Fig 21 : Photon Collection efficiency = F (Focal plane acceptance (deg))
4 TeV Nucleon showers, at 40 m (a) and 70 m (b) from the GIP

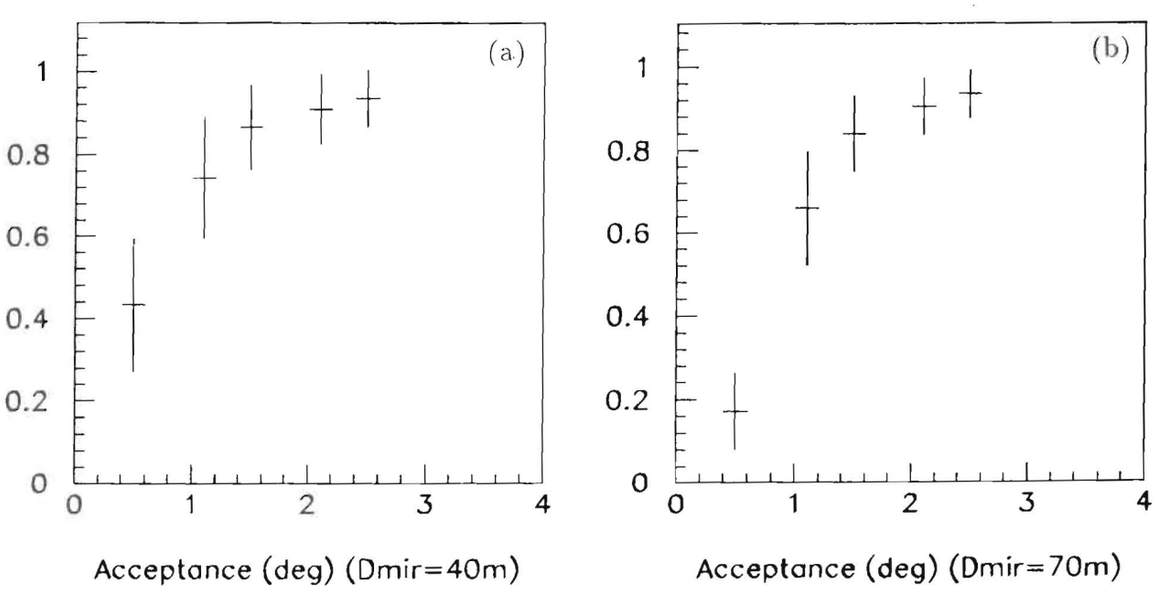

Fig 22 : Photon Collection efficiency = F (Focal plane acceptance (deg))
1 TeV Photon showers, at 40 m (a) and 70 m (b) from the GIP

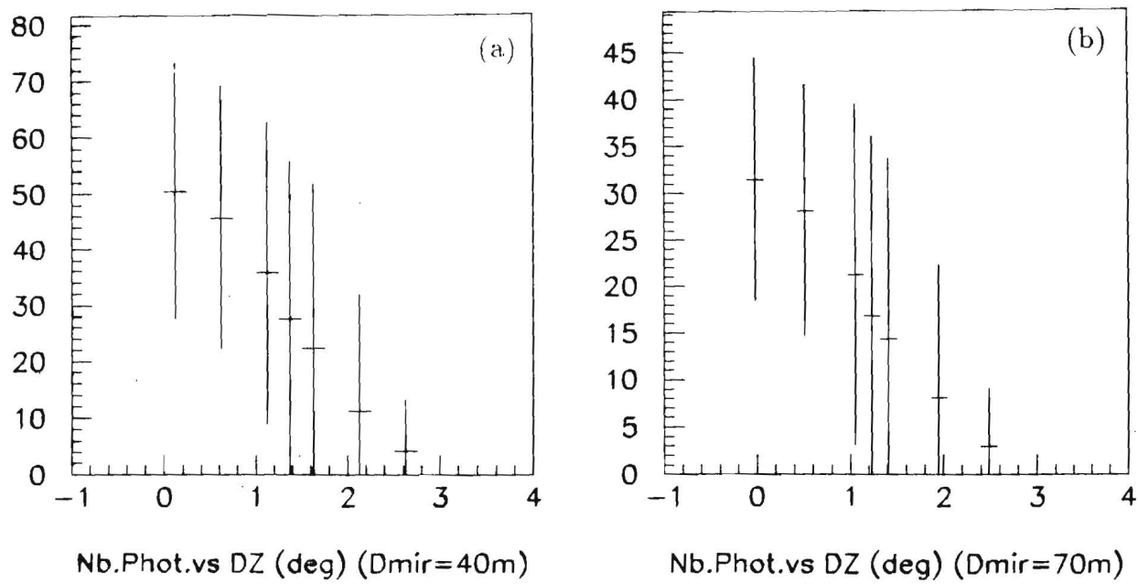

Fig 23 : Number of collected photons as a function of Mirror axis-primary direction offset (deg) for 4 TeV proton showers at 40 m (a) 70 m (b) from the GIP.

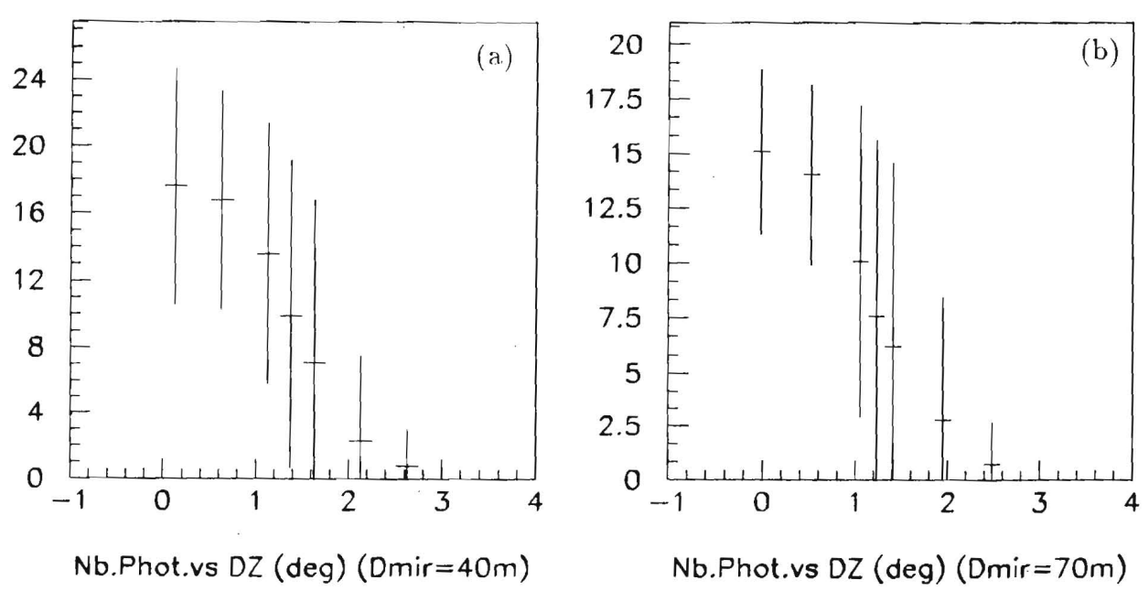

Fig 24 : Number of collected photons as a function of Mirror axis-primary direction offset (deg) for 1 TeV Gamma showers at 40 m (a) 70 m (b) from the GIP.

5 SHOWER IMAGE RECONSTRUCTION

5.1 Method for particle direction determination

The reconstruction of the parent particle direction uses the Cerenkov photons emitted by secondaries mainly by the electrons, in the Extended Air Shower (EAS).

The shower has an elongated shape, with the thrust axis along the parent particle direction. It develops at a mean altitude of $\sim$ 8000 meters and extends over 4000-5000 meters. The lateral extension, perpendicular to the thrust axis is much smaller, and reaches a few hundred meters at ground level. The shower visibility is not limited by the Cerenkov emission angle, due to the rather wide distribution of the secondary particle directions, with respect to the shower axis.

Those photons collected on a spherical mirror give in its focal plane an image whose shape is approximately elliptical. A schematic representatin of a shower-mirror configuration is given in figure 1, where for clarity, the horizontal scale is enhanced by a factor 100 with respect to the vertical one. The exact image of the parent trajectory on the focal plane can be defined by the intersection IF of the plane containing the mirror center and the parent trajectory with the focal plane.

A point (α_x, α_y) in the focal plane of a mirror is the image of a direction in space. On the focal plane, the orthogonal corrdinate system $(O\vec{\alpha}_x, O\vec{\alpha}_y)$ is chosen such that its origin is on the symmetry axis of the mirror. Figure 2.a shows the focal plane coordinate system and notations. The points I and F are the images of the parent direction and the intersection of the parent trajectory with the focal plane respectively. A typical image pattern of a shower in the focal plane is shown in figure 2.b. The image of the parent trajectory in the mirror is identified to the longitudinal axis of a reconstructed ellipse whose equation is :

$$a\alpha_x + b\alpha_y + c = 0$$

That ellipse approximation does not retain any information about the up-down orientation of the shower. The use of a more elaborate asymmetric shape to take into account the smaller lateral extension at the start of the shower developement may reveal such an orientation for a fraction of the events. However such a study goes beyond the scope of the present work where the ellipse approximation will be used throughout.

In the focal plane of the mirror, a detector usually made of photomultipliers, collects the reflected photons within a limited acceptance. Thus the elliptical image may be truncated when recorded. In addition the granularity of the photomultiplier system may also affect significantly the accuracy of the reconstruction. The main factors contributing to the accuracy of the reconstruction are :

a) the shower fluctuations : shape, number of photons

b) the acceptance limitations of the focal plane detector

c) the granularity of the photodetector

5.2 Event generation and selection

The standard mirror setup is described in section 2. As said above the procedure consists in first generating the events and recording with a 12 % efficiency the positions and the angles of the photons which fall on each mirror. The assumed efficiency is taken as the product of the quantum efficiency of the PM's, the reflection coefficient of the mirrors and the filling factor over the area of each detector. Angular acceptances and granularities are introduced at a subsequent stage in the analysis to study their effects on the resolution and on the trigger efficiency.

5.2.1 Event generation

Events are generated for two types of primary particles at several energies. The impact points of the primaries are uniformly distributed over a circular horizontal area of radius 80 m centered at x = y = 0. The bulk of the generation runs are made at a zenith angle of 0° for all the primary particles. Special runs are made with a fixed zenith angle of 30° and 45°.

The mirror axes are aimed in the direction of the primary particles for the runs at fixed zenith angles and in the direction of the average angle for the others. A list of the run conditions and statistics is given in Table 2.

The central mirror information is used to study the Mount Hopkins type of experiment with a single mirror, whereas the properties of a stereoscopic reconstruction are investigated with the same events as viewed in the three other mirrors.

Simulation conditions (primary particle)	Nb. Of Showers
1 TeV Nucleon showers (0° zenith angle)	272
2 TeV Nucleon showers (0° zenith angle)	261
4 TeV Nucleon showers (0° zenith angle)	194
4 TeV Nucleon showers (30° zenith angle)	165
4 TeV Nucleon showers (45° zenith angle)	303
1 TeV Photon showers (0° zenith angle)	137

Table 2: Event samples used for shower reconstruction study (setup with 3+1 10 m. diameter mirrors)

5.2.2 Selection criteria

The selection criteria for the "standard" granularity and acceptance are set as follows:

a) for the photoelectrons (p.e.) within the acceptance of the central region, (± 1.375°), there are at least 3 PM's with more than N_{pe}^{min} and total number of

photoelectrons larger than N_{pe}^{tot}. Two sets of values are used for N_{pe}^{min} and N_{pe}^{tot} :
Low threshold : $N_{pe}^{min} = 5$, $N_{pe}^{tot} = 75$
Standard threshold : $N_{pe}^{min} = 20$, $N_{pe}^{tot} = 300$.

b) the total number N_{pe}^{ext} of photoelectrons within the external ring (angular range 1.375 to 1.875° is such that $N_{pe}^{ext}/N_{pe}^{tot} < 0.6$.

Studies done on data of the Mount Hopkins experiments have shown that, due to the ambiant noise level, the standard threshold set is adequate, whereas the low threshold set would not be. In the case of our study, the low threshold set is deemed necessary to obtain not too low an efficiency for the 1 TeV nucleon events, especially in the case of the stereoscopic reconstruction. For every other generated sample the efficiency obtained with the standard threshold set is considered to be adequate.

The coarser granularity and larger acceptance conditions correspond to the linear dimensions of every detection element and the angular ranges twice as large as for the standard case. The other selection criteria remain unchanged.

5.3 Photoelectron distributions

The distribution of the total number of photoelectrons, N_{tot}, with full angular acceptance and without cuts are shown in figure 25.a and 25.b for nucleons of 1 TeV and of 4 TeV, as primary particles, respectively. As already pointed out in the general shower study, the average numbers of photoelectrons in the two distributions for the nucleons do not scale with the parent energy. As the shower maximum is displaced towards lower altitude as the energy inceases, the accepted solid angle for the Cerenkov photons becomes larger and their attenuation weaker. Both those effects contribute towards an increase of the photon yield per TeV of parent energy. The density distributions $\frac{1}{N}\frac{dN}{dz}$ of the photons collected as a function of the altitude z at which they are emitted are shown on figure 27 for nucleons of 1 and 4 TeV. The altitude corresponding to the maximum of the distribution decreases by 800 m between 1 and 4 TeV, a displacement which is transmitted to the image of the shower.

The distributions of the numbers of photoelectrons, N_{Ver}, within the acceptance of the central detector of radius R = 1.375° are shown in figure 26 for 1 TeV and 4 TeV nucleons, respectively, with a scaling threshold of 75 photoelectrons per TeV. The average accepted fractions relative to the total flux collected by the mirror are 61 % et 1 TeV and 55 % at 4 TeV, a variation which is yet another consequence of the altitude displacement of the shower maximum. The angular acceptance of the mirror being larger at 4 TeV than at 1 TeV, the fraction of photoelectrons within a fixed angular range is smaller.

For 1 TeV gamma parents, the distribution N_{tot} is shown on figure 28.a and that of N_{Ver} with the standard criteria in figure 28.b. The average value of N_{tot} is about twice larger than for nucleons of the same energy and the accepted fraction is 69 %, also larger due to the narrower shower collimation.

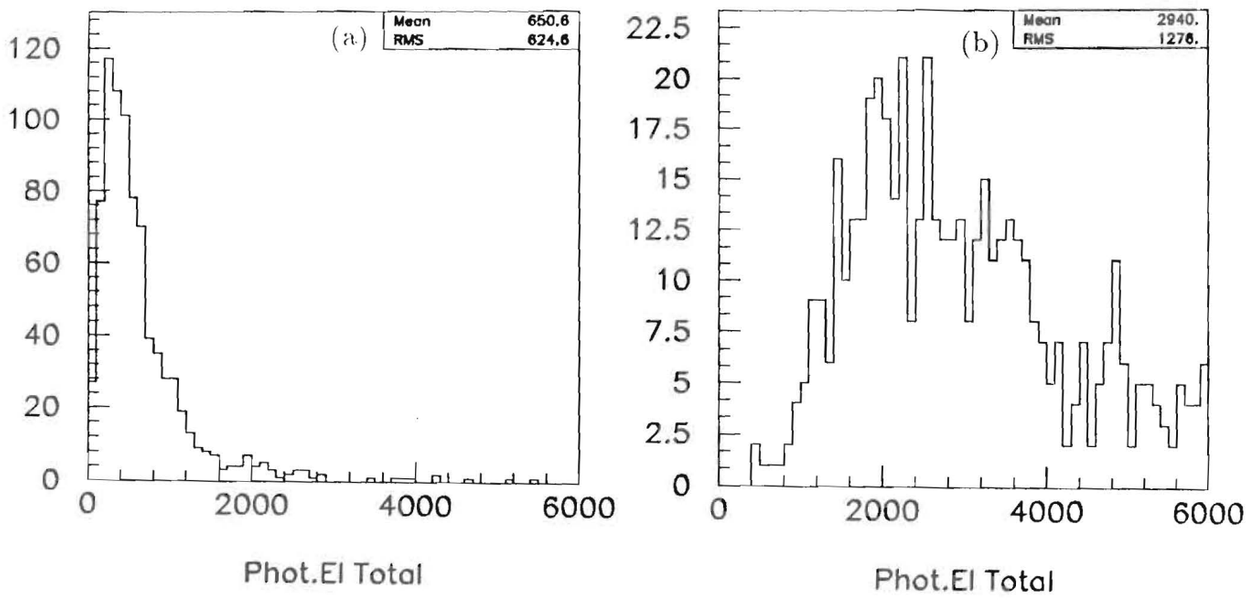

Fig 25 : Total number of photoelectrons N_{tot} for 1 TeV (a) and 4 TeV (b) Nucleon showers

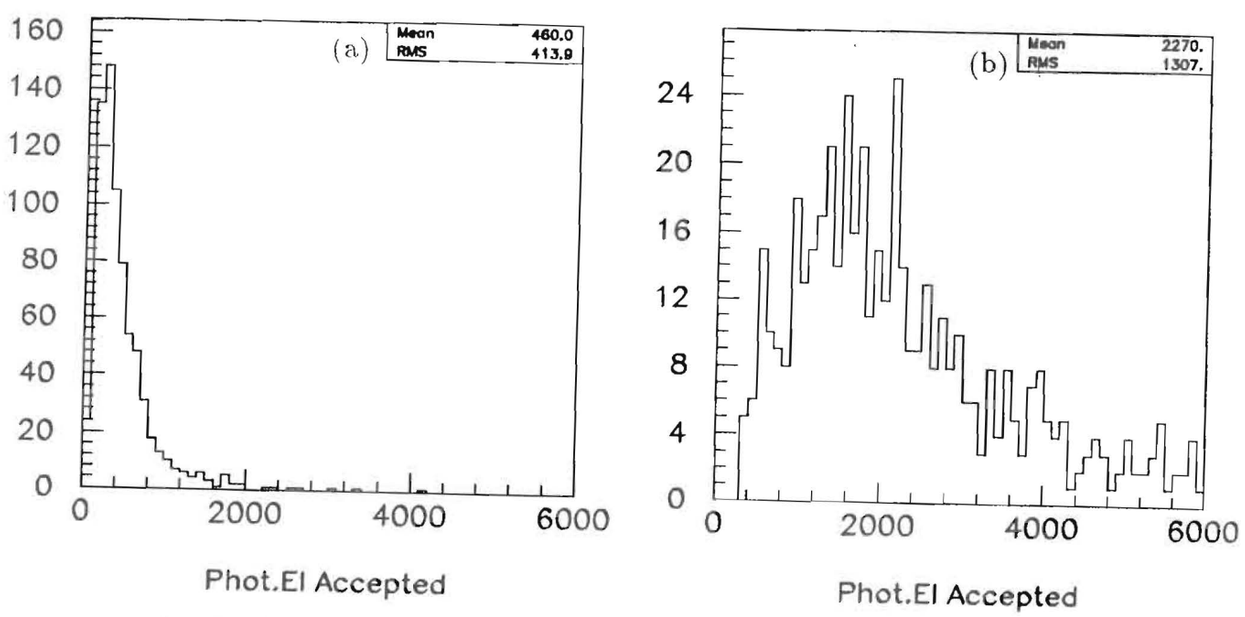

Fig 26 : Number of accepted photoelectrons N_{Acc} for 1 TeV (a) and 4 TeV (b) Nucleon showers

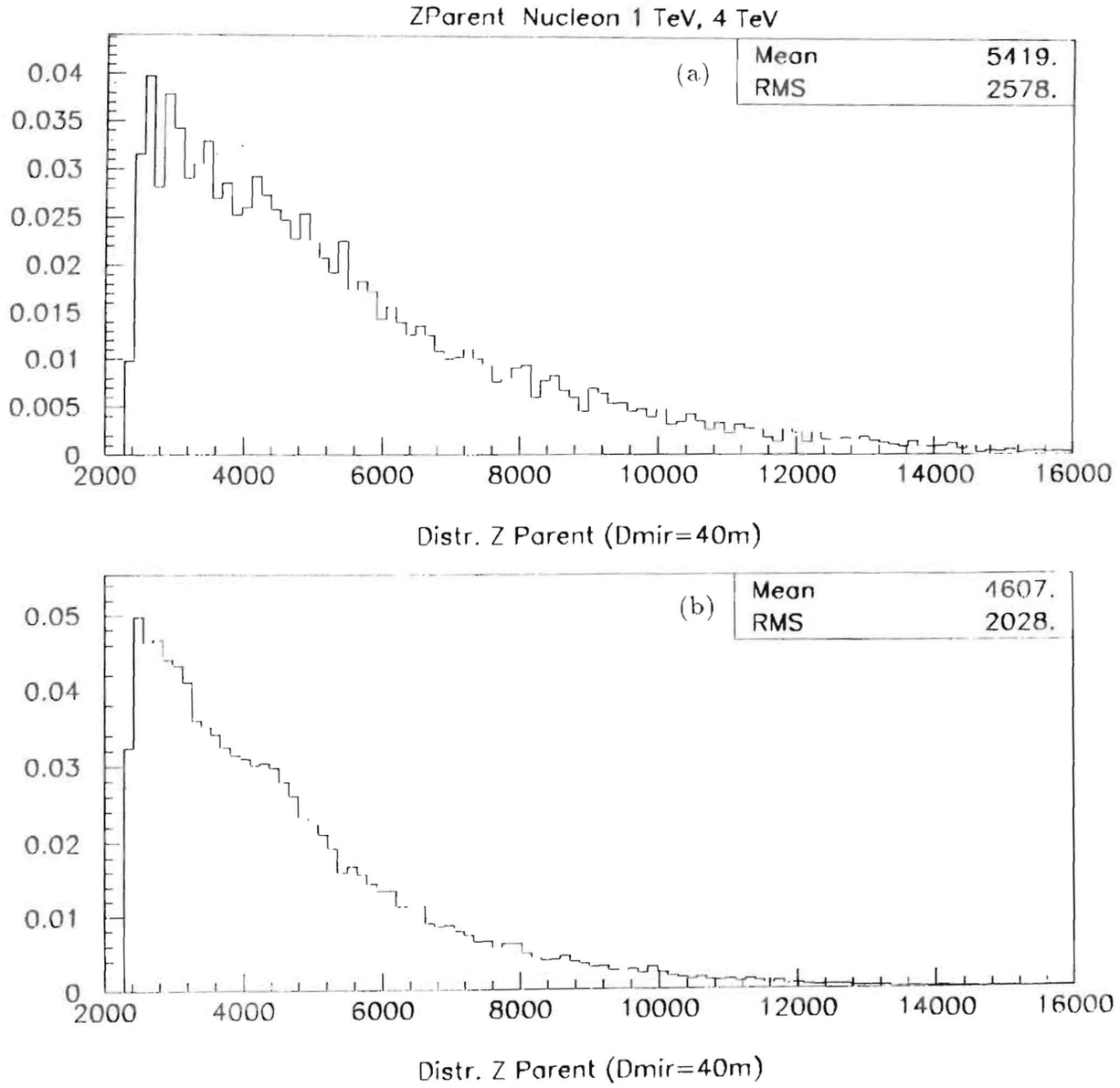

Fig. 27 : Cerenkov photon density distribution $\frac{1}{N}\frac{dN}{dz}$ as a function of emission altitude

(a) 1 TeV Nucleon shower

(b) 4 TeV Nucleon shower

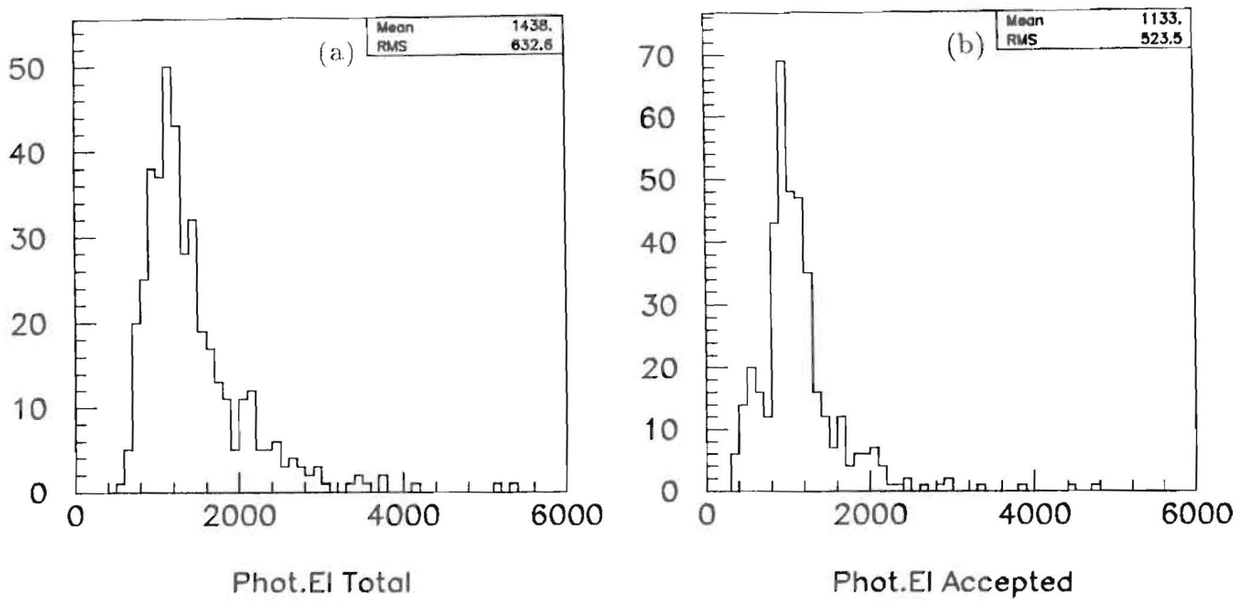

Fig 28 : 1 TeV Gamma showers
N_{tot} (a) and N_{Acc} (b) distributions

5.4 Shower image axis

As noted above, the image of the parent particle trajectory in the mirror focal plane can be identified to the longitudinal axis of the Cerenkov photon pattern over the focal plane. Any ellipse used as an approximation for the shower image in the focal plane is described by 5 parameters (see Fig. 2.a) which are expressed as angles : the coordinates x_G and y_G of its center of gravity G, the half lengths σ_l and σ_t of the longitudinal and transverse axes and the angle θ which defines the orientation of the longitudinal axis. Three basic algorithm are used to compute these parameters :

P_1 every photoelectron contributes with its own weight as given by generation program. The other two algorithms P_2 and P_3 are multistep processes with P_1 as a first step.

P_2 a two step process. For the second step any photoelectron with coordinates α and β with respect to the axes of the initial ellipse such that $\alpha^2/\alpha_l^2 + \beta^2/\alpha_t^2 > 10$ are excluded. The final ellipse parameters are then evaluated.

P_3 a type of algorithm proposed by Hillas. Following the first step, the weight assigned to each photoelectron is multiplied by a factor $1/(1 + d^2/d_0^2)$, where d is its angular distance from the initial ellipse longitudinal axis and $d_0 = 0.1°$. Such an algorithm aims at detecting a hard longitudinal core within the shower as the best means of determining its axis. In practice such an additional weighting procedure was applied as a gradual multistep process to insure a proper convergence.

To compare the reconstructed shower image axis to the exact image of the parent

trajectory (IF), we define the following variables. The notations used are described in figure 2.

- The offset angle ψ between IF and GH, in the focal plane
- The angular distances $d_\perp = IH$ which measures the amount by which the reconstructed axis misses the parent direction (I)
- The angular distance $d_{//} = GH$.

The offset angle ψ can be related to the space angle measurement error (α) on the parent particle direction by geometrical factors :

$$tg\alpha \simeq \frac{D_{Mir-GH}}{h} tg\psi$$

where D_{Mir-GH} is the mirror-ground impact point distance and h is the mean shower altitude above the observation level. Typically tgψ is about 100 times larger than tgα for small values of α.

5.5 Accuracy of the reconstructed axis

For this part of the study, the event samples are such that the mirror axis is parallel to the parent direction. The angular coordinate of that direction in the focal plan are thus ($\alpha_x = 0, \alpha_y = 0$).

The shortest distance $d_\perp$ between the origin and the ellipse axis is used to characterize the projected angular offset of the reconstructed shower axis.

The effects of the angular acceptance and the granularity are first studied with the 4 TeV nucleon shower sample generated at 0° zenith angle.

5.5.1 Effect of the Detector Angular Acceptance

That first part of the study is made assuming an infinitely fine granularity. There are no selection criteria specific to the analysis without granularity. However, unless otherwise specified, only the events included into the corresponding granularity sample are retained for these analyses in order to perform a meaningful comparison. The distributions of $d_\perp$ are shown for the three types of weights for

i) the standard angular acceptance (1.375°, 1.875°) for the limits of the two angular regions in figure 29.

ii) the larger angular acceptance (2.75°, 3.75°) in figure 30.

The accuracy improves for all the weight types at the larger acceptance. A comparison between figure 30.a and figure 30.b shows that the exclusion of the excentric photons for the ellipse determination improves the accuracy for the larger acceptance, although that does not appear to be the case for the standard acceptance. The weighting procedure P_4 of the type proposed by Hillas, figure 29.c and 30.c, gives good results even at small acceptance.

The angular size of the shower is large compared to the standard acceptance, which leads to strong alteration of the image shape. However even under such conditions the Hillas weighting procedure is capable of detecting a hard longitudinal core within the shower, giving a better axis determination than the other procedures.

5.5.2 Effect of the granularity

The $d_\perp$ distributions are shown for the 4 TeV nucleon sample for the standard granularity and acceptance in figure 31 for the P_2 and P_3 weighting procedures, respectively. The corresponding distributions for the coarse granularity are shown on figure 32. The comparison with the figures of the previous paragraph show that the effect of the granularity is more important for the weight P_3 than for P_2. The detection of a hard longitudinal core within the shower (P_3) is spoiled due to the granularity smearing and the accuracies for the two types of weights become comparable. In what follows only the weight P_3 will be used.

5.5.3 Energy and parent type dependances of the accuracy

The $d_\perp$ distributions are shown for the standard granularity and acceptance in figure 33 for 2 TeV and 1 TeV nucleons and in figure 34 for 1 TeV gammas, respectively.

For nucleons, comparing to the distribution at 4 TeV of figure 31.c, the resolution gets worse at lower energies, as expected. For 1 TeV gammas the resolution is much better than for nucleons due to the smaller angular extension of the gamma shower.

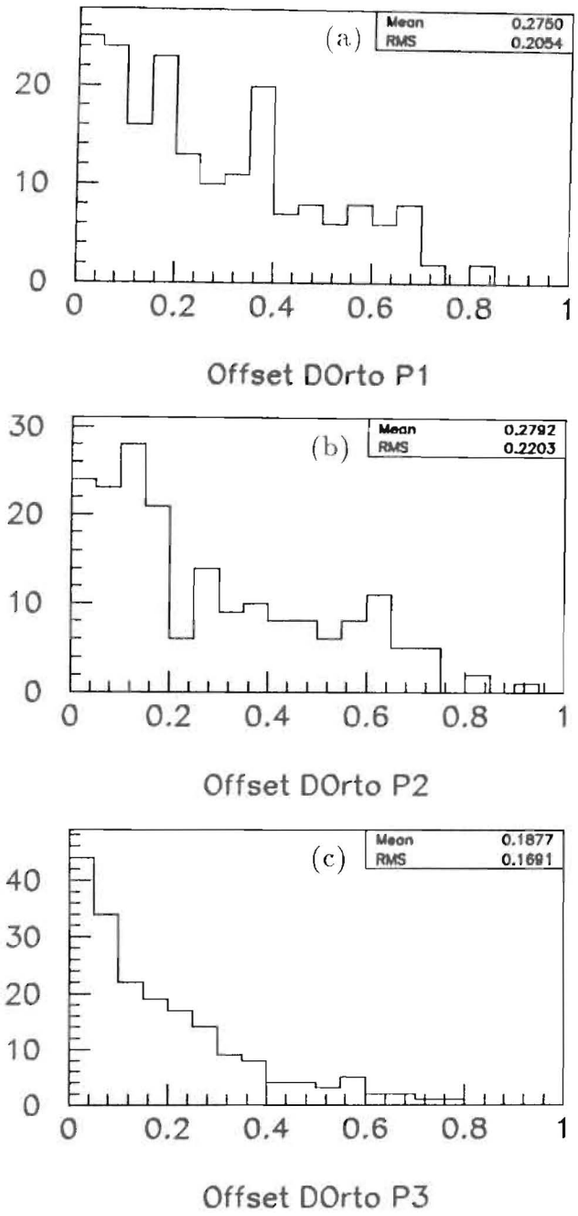

Fig 29
Standard angular acceptance
(1.375°/1.875°)

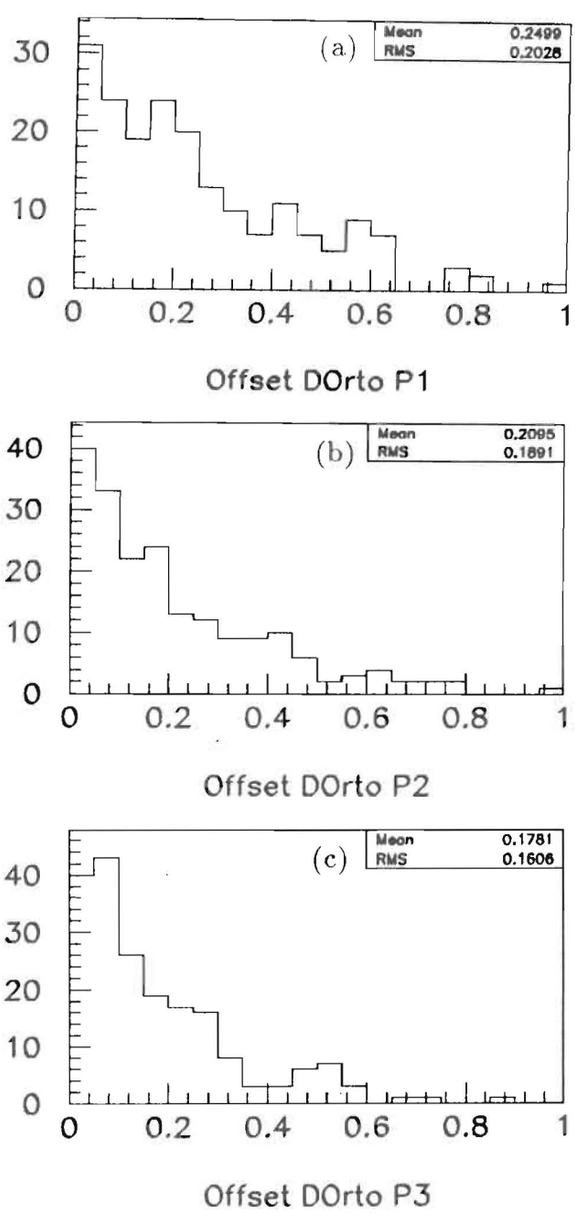

Fig 30
Large angular acceptance
(2.75°/3.75°)

$d_\perp$ distribution for 4 TeV Nucleon showers.
No granularity for P_1 (a), P_2 (b), P_3 (c) weighting procedures

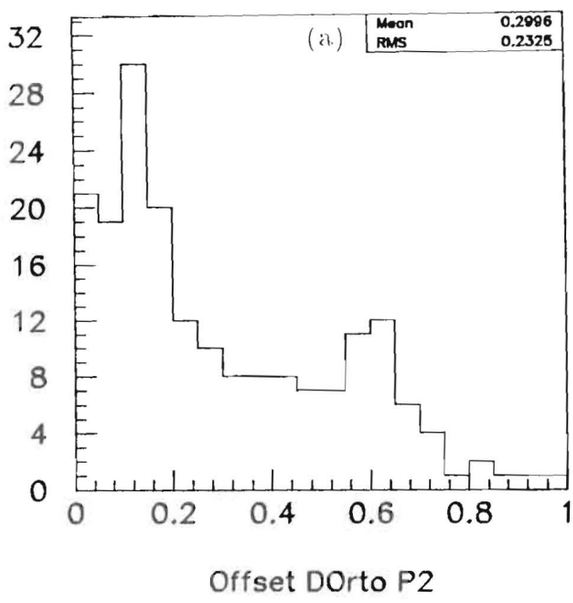

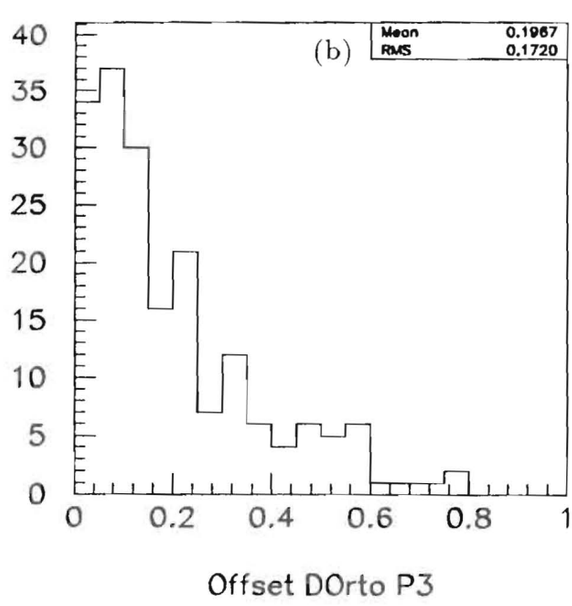

Fig 31
Standard acceptance/granularity

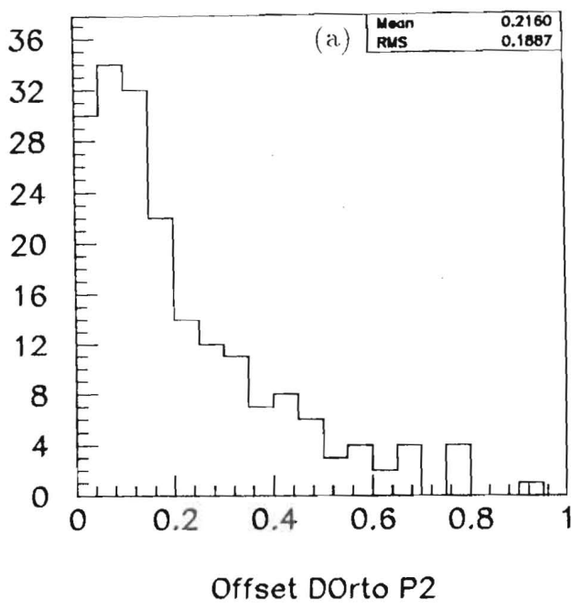

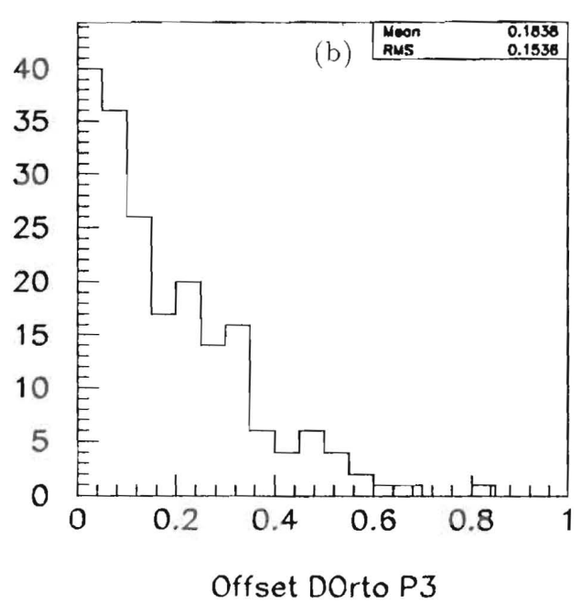

Fig 32
Large acceptance/Coarse granularity

d_L distribution for 4 TeV Nucleon showers.
P_2 (a), P_3 (b) weighting procedures

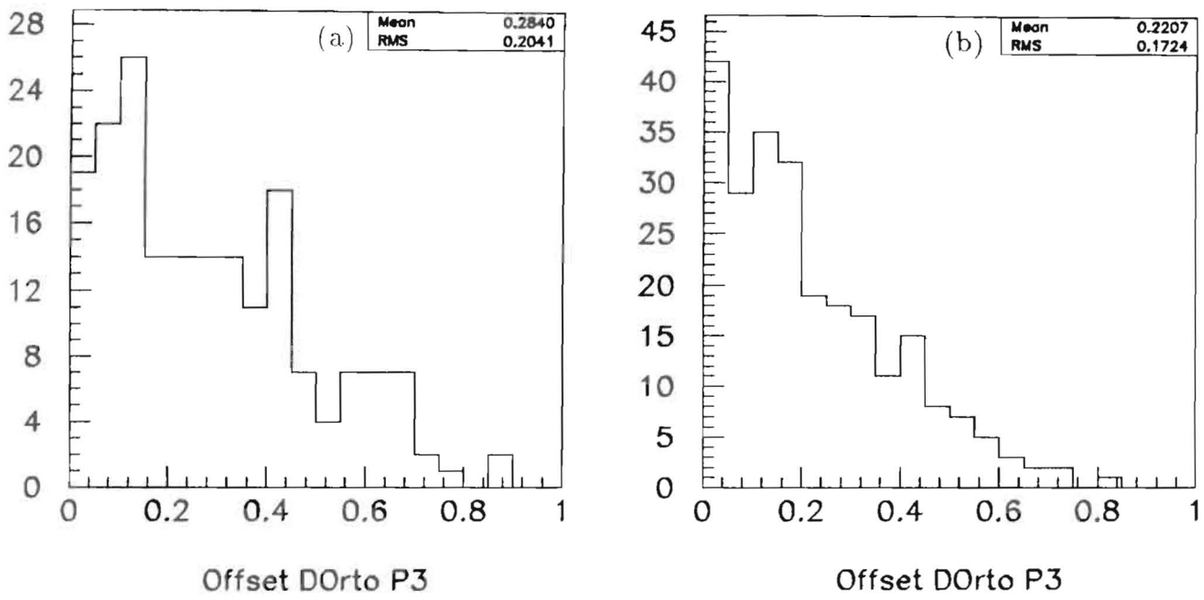

Fig 33 : $d_\perp$ distribution (standard acceptance/granularity)
P_3 weighting procedure
(a) 1 TeV Nucleon showers
(b) 2 TeV Nucleon showers

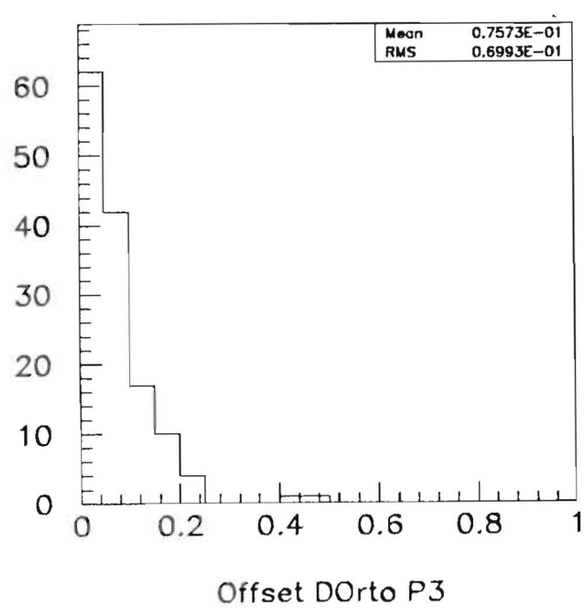

Fig 34 : $d_\perp$ distribution (standard acceptance/granularity)
P_3 weighting procedure - 1 TeV Gamma showers

6 RECONSTRUCTION OF THE PARENT PARTICLE DIRECTION

The direction of the parent particle is reconstructed from the stereoscopic images of shower axis obtained from two mirrors at least. The mirror setup used for the simulation is that described in section 2.2 : three mirrors, 10 meters in diameter, positionned such that their centers are 120 m apart in an equilateral triangle configuration. The axes of the mirrors are all pointing in the same direction. That is an example of what might be a multimirror setup.

Both the parent particle and the mirror axis directions were at a zenith angle of 0° for the event samples of the single mirror study presented above. For the multimirror study, in addition to those same events viewed by several mirrors, two new samples of 4 TeV nucleon showers with zenith angles of 30° and 45° respectively, are included. For both of these new samples the mirror axes are parallel to the parent particle directions. In addition the 4 TeV nucleon and the 1 TeV gamma 0° samples are used to generate uniformly distributed parent particle directions within a cone of half angle 1.5° around the mirror axes direction. In that way the detector properties averaged over a finite solid angle of about $2.2\ 10^{-4}$ steradians are also studied.

6.1 Reconstruction Efficiencies

The selection criteria are those listed in section 5.2. For all the event samples, the standard granularity, acceptance and thresholds are used. In addition, for the 1 TeV nucleon sample alone, a low set of threshold, as defined in section 5.2, is also used.

The detection efficiencies are listed in table 3 for the various event samples. The nucleon shower efficiency increases rapidly with the parent energy. With the mirror axes pointing in the parent direction at 0° zenith angle, the two mirror efficiency for the standard criteria which is only 43 % at 1 TeV reaches 69 % at 2 TeV. However due to the small angular acceptance of the detector, the efficiency decreases fast as the angle of the parent particle direction with respect to the mirror axis becomes larger. The two mirror efficiencies averaged over a half angle of 1.5° are down by about a factor of 2 with respect to the 0° efficiencies. For the showers originating from gamma parents the 0° are already almost 100% at 1 TeV, due to the slimmer angular size of the showers and their large photon yield per TeV compared to nucleon showers. However the efficiency drop as a function of the angle between the parent particle and the mirror axis directions is as fast as for nucleon showers.

For 4 TeV nucleon showers at large zenith angles (45° and 30°), and with the mirrors pointing in the parent particle direction, the efficiencies remain high with respect to those of nucleon showers of the same energy at zero degree zenith angle, in spite of the larger atmospheric absorption. This effect is coupled with a resolution steadily improving as the shower inclination increases and will be discussed later.

Simulation conditions	(a)	(b)	(c)	(d)
(1) 4 TeV Nucleon 0° Standard granularity/Acceptance	97 %	81 %	92 %	70 %
(2) 4 TeV Nucleon 0° Coarse granularity/Large Accept.	100 %	98 %	100 %	97 %
(3) 2 TeV Nucleon 0° Standard granularity/Acceptance	94 %	75 %	88 %	65 %
(4) 1 TeV Nucleon 0° Standard granularity/Acceptance High Thresholds	69 %	31 %	44 %	22 %
(5) 1 TeV Nucleon 0° Standard granularity/Acceptance Low Threshold	97 %	77 %	91 %	68 %
(6) 1 TeV Photon 0° Standard granularity/Acceptance	100 %	92 %	97 %	85 %
(7) 4 TeV Nucleon 30° zenith angle Standard granularity/Acceptance	98 %	88 %	95 %	81 %
(8) 4 TeV Nucleon 45° zenith angle Standard granularity/Acceptance	99 %	97 %	98 %	97 %
(9) 4 TeV Nucleon 0° zenith angle Random Mirror axis offset – Max ± 1.5° Standard granularity/Acceptance	54 %	28 %	43 %	17 %
(10) 4 TeV Nucleon 0° zenith angle Random Mirror axis offset – Max ± 1.5° Large Acceptance, No Granularity	99 %	94 %	99 %	92 %
(11) 1 TeV Photon at 0° zenith angle Random Mirror axis offset – Max ± 1.5° Large Acceptance, No Granularity	63 %	35 %	54 %	27 %
(12) 1 TeV Photon at 0° zenith angle Random Mirror axis offset – Max ± 1.5° Large Acceptance, No Granularity	98 %	98 %	100 %	97 %

Table 3 : Selection efficiencies

(a) Single mirror setup
(b) 2 mirror setup (2 reconstructed ellipses)
(c) 3 mirror setup ($\geq$ 2 reconstructed axis ellipses)
(d) 3 mirror setup (3 reconstructed ellipses)

6.2 Accuracy of the space angle reconstruction

As for the single mirror case (5.4), the image of the shower axis in the n^{th} mirror is the reconstructed axis of the ellipse for that mirror :

$$a_n\ \alpha_r + b_n\ \alpha_y + c_n = 0$$

As the axes of all the mirrors point in the same direction, the images of the parent direction have the same coordinates (α_r^I, α_y^I) for all the three mirrors.

For the events where the ellipse longitudinal axis are available for only two of the three mirrors, the reconstructed parent direction is simply the intersection between those two axes. If the ellipse axes are available for all the three mirrors, the reconstructed parent direction is the average between the coordinates of the three axis intersections, weighted according to the angle between the axes.

6.2.1 Vertical showers

The offset angle Δ of the reconstructed parent particle with respect to its true direction, and its components (Δ_r, Δ_y), are used as a measure of the space reconstruction accuracy. The distributions of Δ, Δ_r and Δ_y are shown on figures 35-38 for the 4 TeV nucleon sample at 0° zenith angle for several detector configurations. The weight type P_3 is applied in all the cases. For figure 35 the standard acceptance and granularity are used, whereas figure 36 corresponds to a two times larger angular acceptance and a coarser granularity. The figures 37 and 38 show the results obtained with the same two angular acceptances defined in section 5.2, but with an infinitely fine granularity. The average values of Δ range from a high 0.49° (Fig. 35) to a low 0.24° (Fig. 38). Such changes in the space reconstruction accuracy follow closely those observed with the quantity $d_\perp$ in the single mirror case. The accuracy gets better with a larger angular coverage. In addition an important effect with the weight P_3 is the improvement of the resolution for the infinitely fine granularity configurations. As in the single mirror case that is due to the detection of a narrow hard longitudinal core within the shower, which the P_3 weighting procedure has been designed to emphasize. The average values of Δ for the 4 TeV nucleon sample at 0° zenith angle in each of the four configurations used above and for each of the weighting procedures P_2 and P_3 are shown on figure 39. Although the values of the reconstruction accuracies are comparable for the two weighting procedures in the finite granularity configurations, the accuracy is better with P_3 than with P_2 in the no-granularity configurations due to the detection of the shower core.

The distributions of Δ for all the other 0° zenith angle shower samples nucleons 1 and 2 TeV and gammas 1 TeV are shown on figure 40 and figure 41 for the standard threshold, acceptance and granularity conditions. The nucleon distributions deteriorate at lower energies. The determination of the parent direction for 1 TeV Gammas is much more accurate than for nucleons due to the smaller lateral extension of the shower.

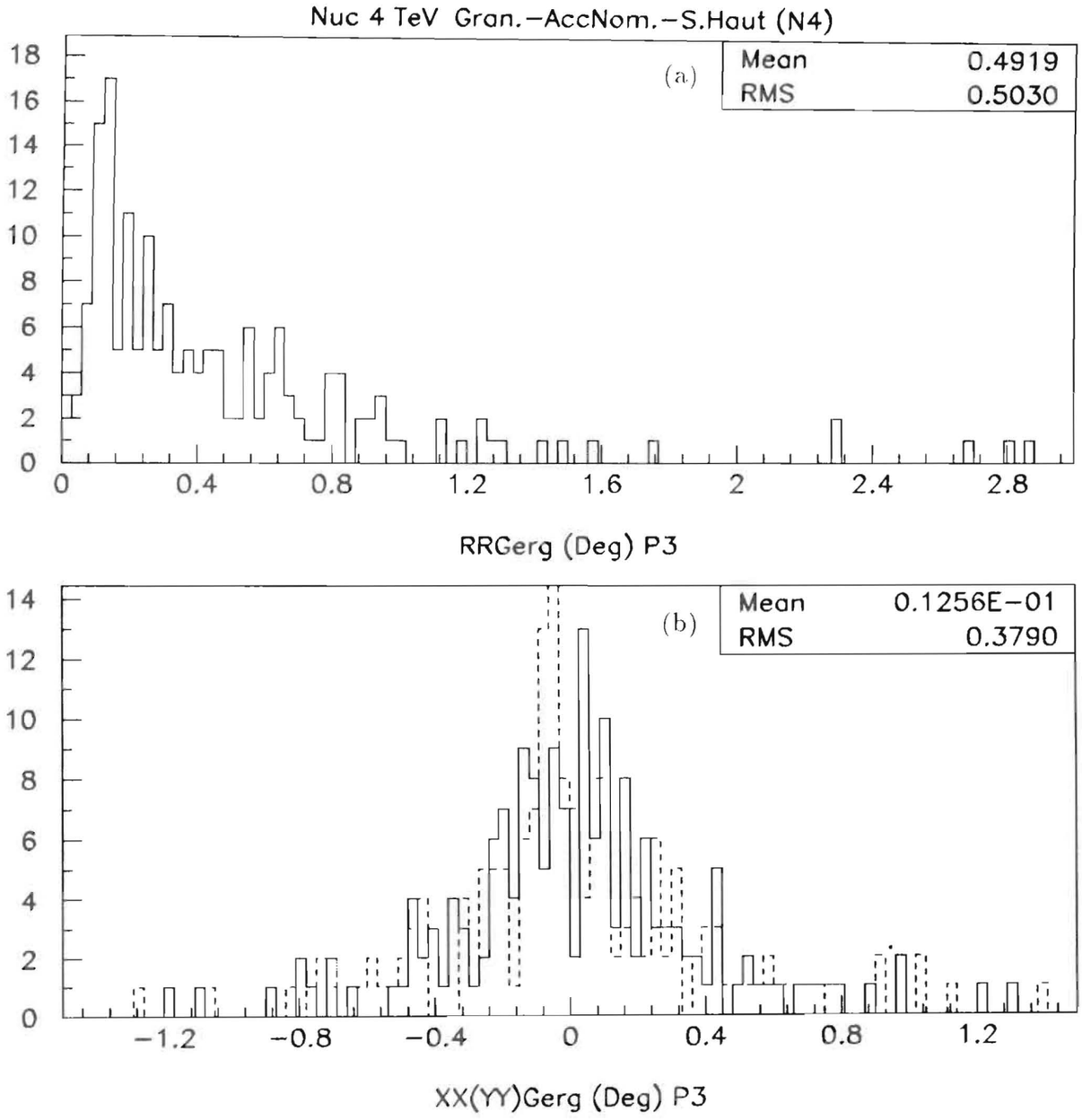

Fig 35 : Δ (a) $\Delta x/\Delta y$ (b) distribution P_3 (Degree)
4 TeV Nucleon showers - Standard acceptance / granularity

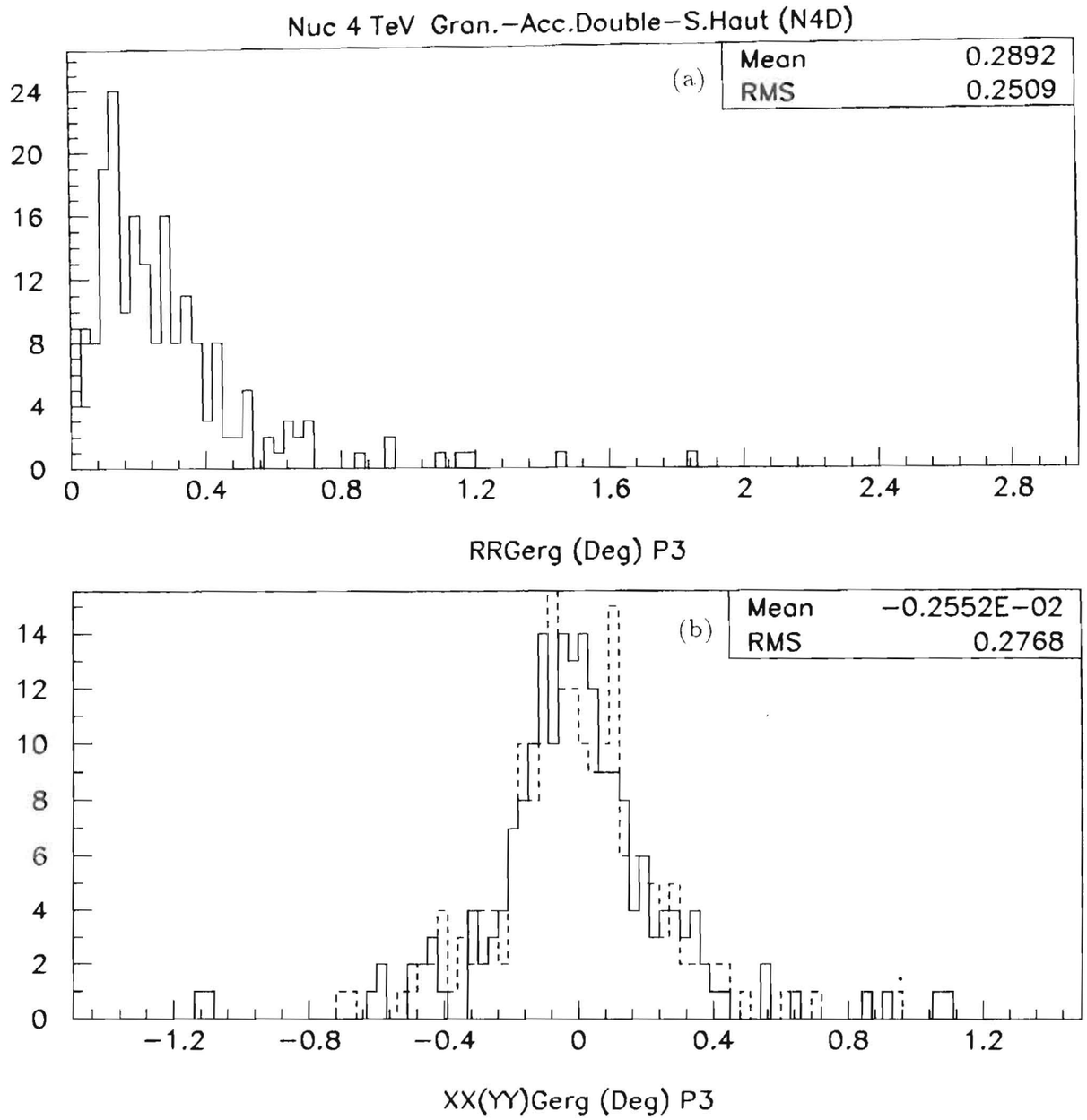

Fig 36 : Δ (a) $\Delta x/\Delta y$ (b) distribution P_3 (Degree)
4 TeV Nucleon showers - Large acceptance / Coarse granularity

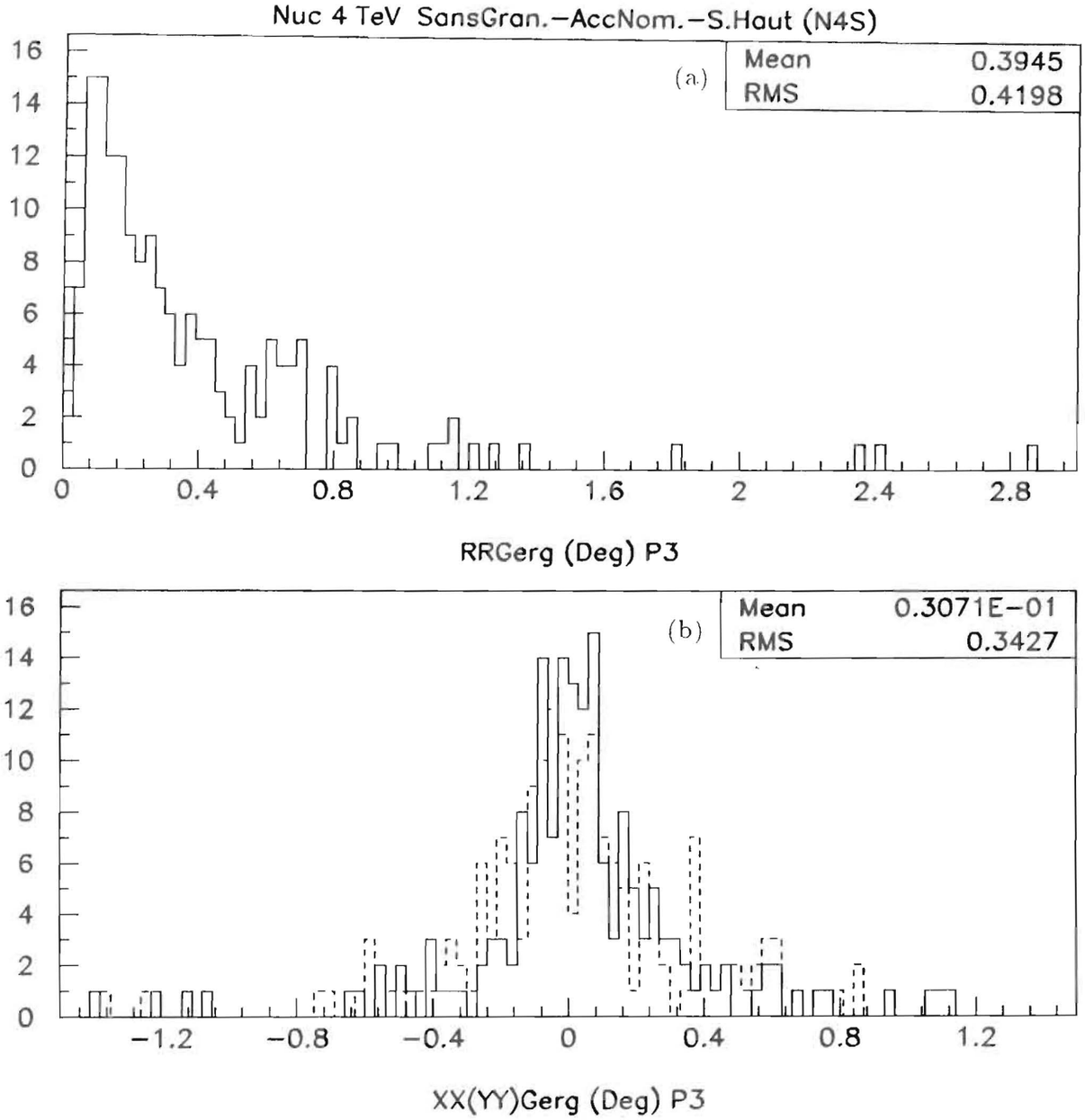

Fig 37 : Δ (a) $\Delta x/\Delta y$ (b) distribution P_t (Degree)
4 TeV Nucleon showers - Standard acceptance / No granularity

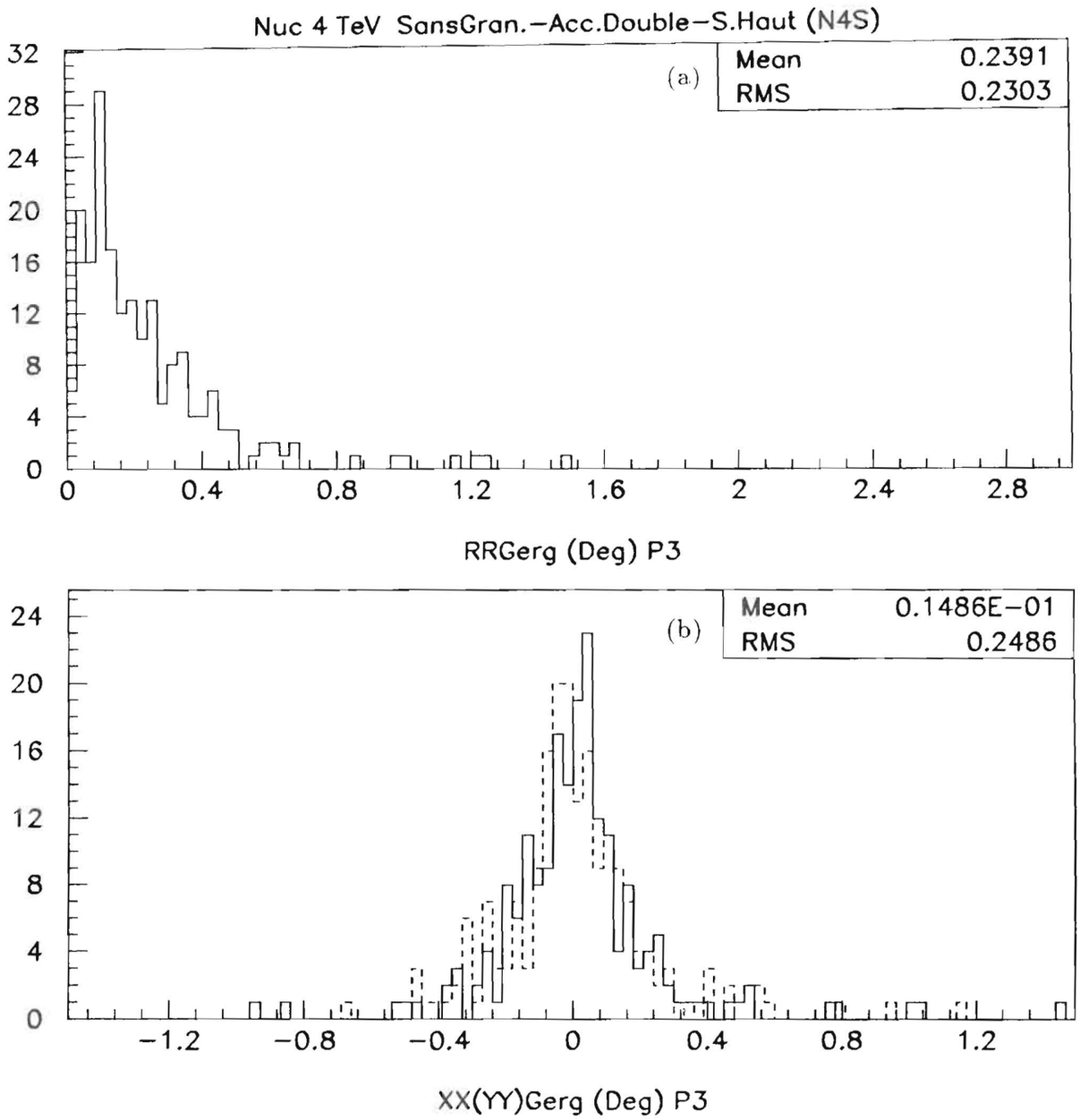

Fig 38 : Δ (a) $\Delta x/\Delta y$ (b) distribution P_3 (Degree)
4 TeV Nucleon showers - Large acceptance / No granularity

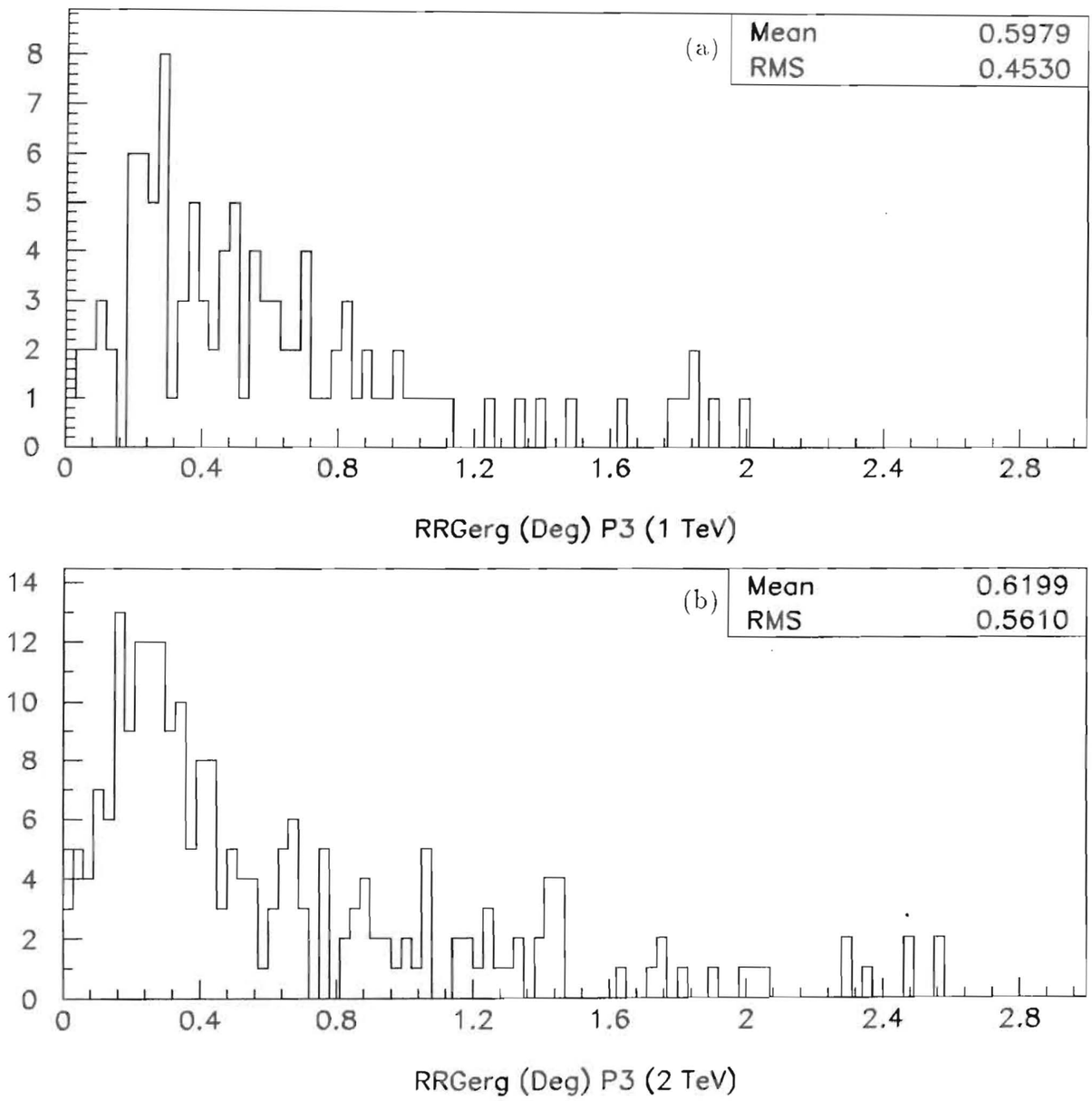

Fig 10 : 1 TeV (a) and 2 (b) TeV Nucleon showers
Δ distribution P_3 (Standard acceptance / granularity)

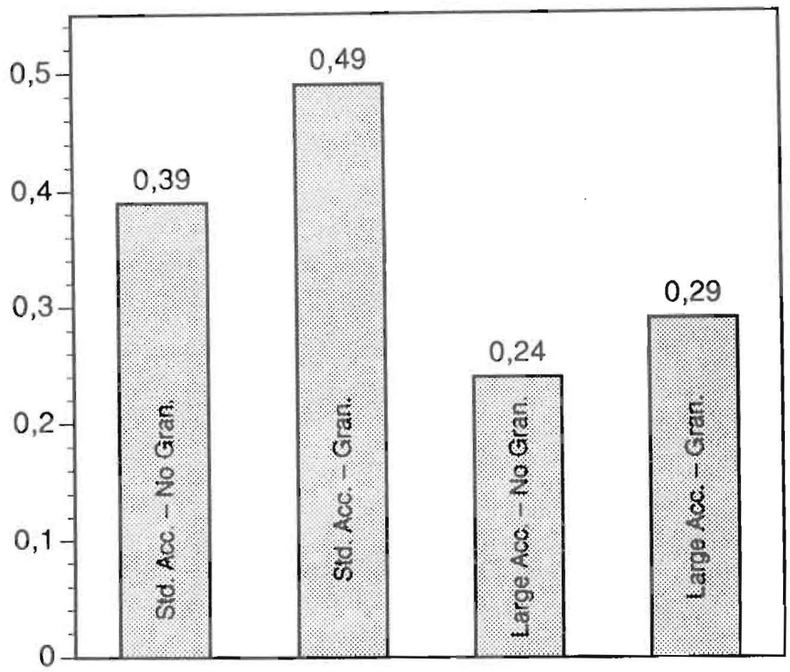

Fig 39 : Mean Δ values for different configurations (4 TeV Nucleon)

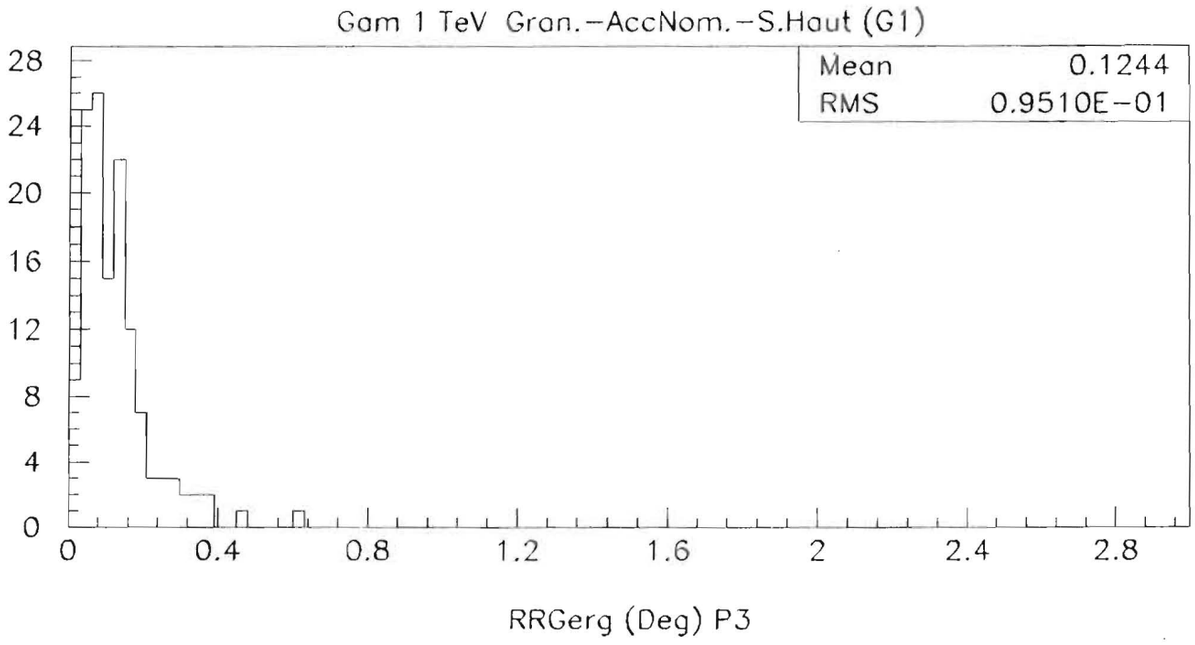

Fig 41 : 1 TeV Photon showers
Δ distribution P_3 (Standard acceptance / granularity)

6.2.2 Inclined showers

The distributions of Δ for the 4 TeV nucleon samples at zenith angles of 30° and 45° are shown on figure 42.a and 42.b, respectively. The mirror axes aim at the parent direction in both cases. The standard thresholds and acceptance and the P_3 weighting procedure are used.

The space reconstruction accuracy improves at larger zenith angles. For the same values of the other parameters, the average of Δ which is 0.49° at 0° zenith angle (Fig. 35) takes the value 0.29° at 45° (Fig. 42.b).

The improvement of the resolution is due to the combination of several effects. Inclined showers ($\theta \neq 0$) develop at higher altitudes than vertical showers ($\theta = 0°$), as there is a $1/\cos\theta$ multiplicative factor for the amount of material traversed. The density of the atmosphere, and therefore the Cerenkov angles are smaller at higher altitudes. Also, due to the larger distance between the mirrors and the shower core ($\sim$ factor 2 at 45° compared to $\theta = 0°$), low energy particles with widely spread directions cannot illuminate the mirrors located close the primary ground impact point ($\sim$ 100 m). As a result, there is a natural angular collimation of the collected Cerenkov photons, leading to an improvement of the parent direction determination accuracy.

But as the photon path length increases, the photon absorption becomes also larger. This additional attenuation amounts to a factor 2 at a zenith angle of 45° for photons in the visible range. Also, as it was noted above, the contribution of Cerenkov photons from low energy secondaries, which are close to the ground in the case of vertical nucleon showers is suppressed.

These low energy particles are responsible for the large photon yields of nucleon showers close to the ground impact point (d $\lesssim$ 30-40 m) as well as the increased lateral size of the shower image. The net effect is a decrease in the photon yield as the zenith angle increases. The detection energy threshold increases correspondingly. However, the selection efficiency stays high due to smaller lateral image size and the accuracy of the parent direction reconstruction improves.

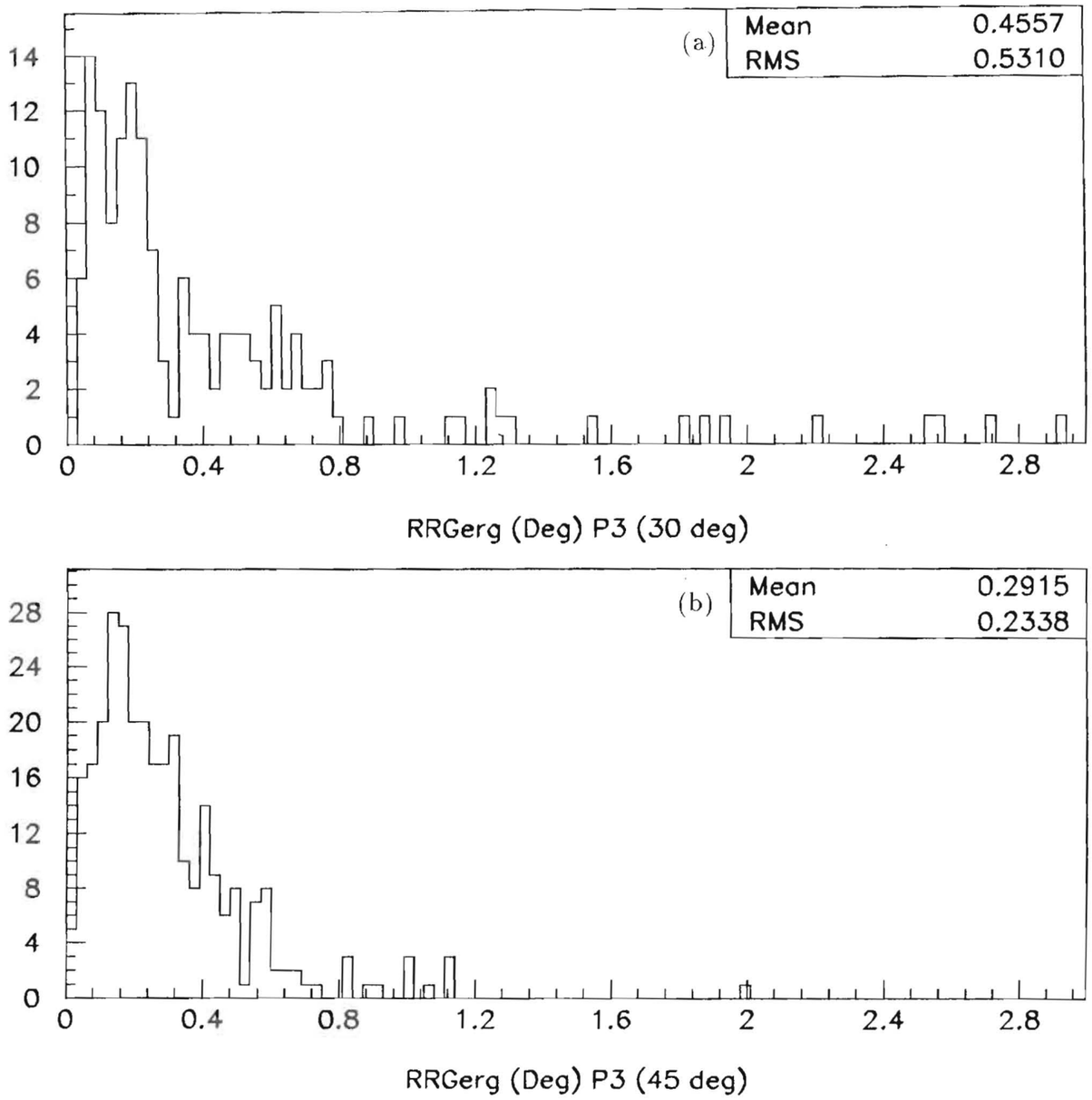

Fig 42 : 4 TeV Nucleon - Δ distribution P_3 (Standard acceptance / granularity)
(a) at 30° zenith angle
(b) at 45° zenith angle

6.2.3 Off Axis Parent Particles

In the previous sections we have only discussed the angular resolutions for configurations with parent particle directions parallel to the mirror axes. As discused in section 6.1, the efficiencies decrease rapidly when the parent particle makes an angle with the mirror axes due to the limited angular acceptance. In addition the resolution deteriorates rapidly for the accepted events. The distributions of Δ for uniformly distributed parent particle directions within a cone of half angle 1.5° around the mirror axes direction are shown in figure 43 and figure 44 for 4 TeV nucleons and 1 TeV gammas, respectively. The standard thresholds, acceptance and granularity are used. A comparison with figure 35 and figure 41 shows the deterioration of the resolution in both cases. The distributions of Δ for the 1 TeV nucleon and the 1 TeV gamma samples for a twice larger angular acceptance and an infinitely fine granularity, are shown on figure 45 and figure 46, respectively. The resolution improves by a factor 2 in both cases.

For gamma parents, telescope setups are used in searches of point like sources with negligeable angular dispersion. On the contrary in most applications parent nucleons have wide angular distributions.

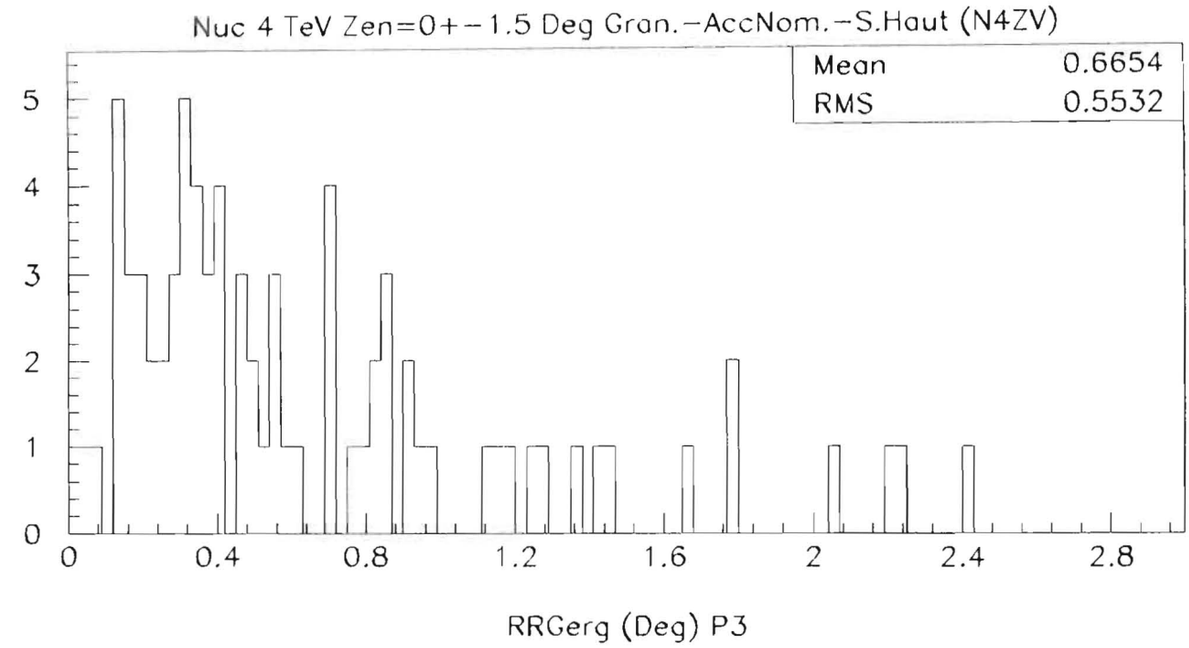

Fig 43 : Δ distribution P_4 (Standard acceptance / granularity)
4 TeV Nucleons with random mirror axis offset (Max $\pm 1.5°$)

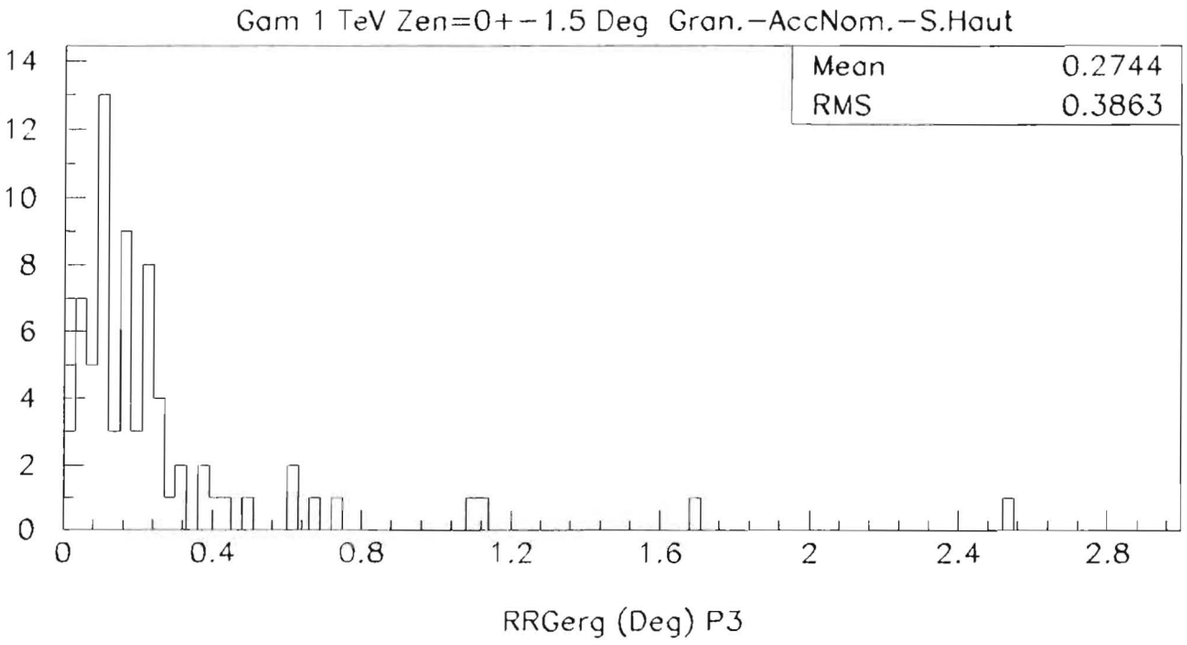

Fig 44 : Δ distribution P_4 (Standard acceptance / granularity)
1 TeV Photons with random mirror axis offset (Max $\pm 1.5°$)

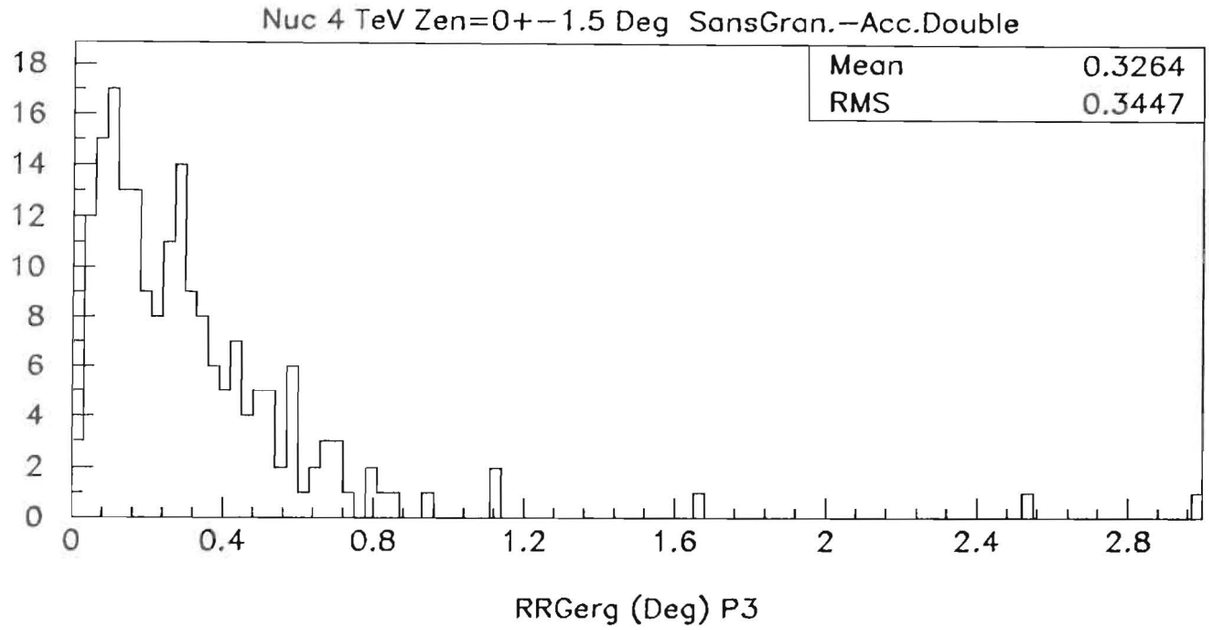

Fig 45 : Δ distribution P_3 (Large acceptance / No granularity)
4 TeV Nucleons with random mirror axis offset (Max $\pm 1.5°$)

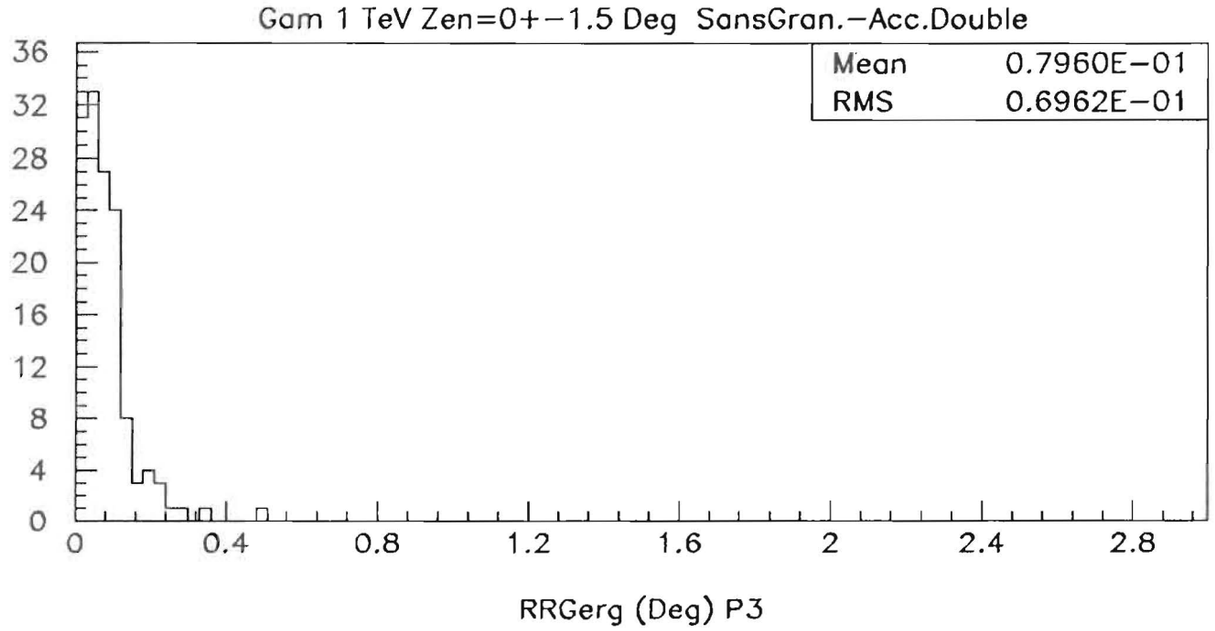

Fig 46 : Δ distribution P_3 (Large acceptance / No granularity)
1 TeV Photons with random mirror axis offset (Max $\pm 1.5°$)

7 CONCLUSION

A study of the detection and the measurement using Cerenkov imaging techniques of showers produced by cosmic ray in the atmosphere has been presented. The MOCCA Montecarlo generator has been used for the simulation of nucleon showers with energies in the TeV range (1-4 TeV) as well as for 1 TeV photon showers, with Cerenkov photons in the visible range. The MOCCA generator is now available at the IN2P3 computing center. Extensive checks, including the study presented here, show that the MOCCA generator is a reliable tool for the simulation of very high energy cosmic ray showers, in the TeV range and above.

Although muon production may be underestimated in the present simulations, the results presented in this paper show little sensitivity to a muon rate within reasonable limits.

We summarize here the main results of our study. First the collection of enough Cerenkov photons for showers in the TeV energy range to reconstruct the shower parameters call for large mirrors, typically 10 meter in diameter or larger. Furthermore, the angular acceptance of the focal plane plays an important role for the accuracy of the image axis determination, especially in the case of nucleon showers. An angular coverage of at least $\pm 2^\circ$ with respect to the mirror axis is needed for an acceptable containement of the shower image. Even for a sizeable angular acceptance the accuracy of the shower axis determination deteriorates rapidly as a function of the angle of the cosmic ray with the mirror axis. The reconstruction accuracy is less sensitive to the granularity of the photon detector, unless a very fine granularity is used thus allowing the detection of a central hard core in the shower.

For 4 TeV nucleon showers an accuracy of about $\pm 0.5^\circ$ on the reconstructed nucleon direction is obtained with our "Standard" setup. That setup is composed of three 10 meter diameter mirrors, with focal planes equipped with 1" PMT's for angles up to 1.4° with respect to the mirror axis and with 2" PMT's for larger angles up to 1.9°. The accuracy of the primary direction improves to 0.29° if both the focal plane coverage and the detector granularities are made larger by a factor 2. If a very fine granularity is used the accuracy is 0.39° and 0.24°, in the cases of standard and of the larger acceptances, respectively. For 1 TeV photons, with the standard setup, the accuracy is 0.12°, about 4 times better than for 4 TeV nucleon in the same setup.

All the values given above refer to the best case with the cosmic ray direction parallel to the mirror axis. For finite angles between these directions, the error on the primary direction increases significantly and the detection efficiency decreases. For a sample of cosmic rays distributed isotropically within a cone of half angle 1.5° around the mirror axis direction, the accuracies become 0.66° for 4 TeV nucleon showers and 0.27° for 1 TeV gamma showers. Beyond 1.5° the detection efficiency is very small.

Acknowledgments

We would like to thank M. Urban, P. Fleury, and E Pare for very useful discussions. A.M. Hillas has provided us with the shower Montecarlo generator (MOCCA). His advice has guided us throughout this work.

Appendix A : ARTEMIS EXPERIMENT

The amount of primordial antimatter from other galaxies in cosmic rays is an important issue for models of the Universe. However backgrounds due to secondaries make searches for such antimatter sensitive only for energies $\geq$ 1 TeV. A discussion of this subject, as well as a summary of the $\bar{p}/p$ ratio measurements in cosmic rays can be found in references [13] and [14].

$\bar{p}/p$ ratio measurements, up to 10-20 GeV energy have been performed mainly with magnetic spectrometers aboard sattelite or balloon experiments. The extension of these measurements to higher energies requires a larger magnetic bending power, ($\int B.d\ell$) combined with a much larger detector acceptance, to cope with the exponential decrease in cosmic ray flux. Direct detection seems thus excluded, given the weight and size limitation of spatial experiments.

The key ideas of the ARTEMIS [1], [2] experiment are :

The use of the earth magnetic field for the spectrometer. This field, although weak in magnitude ($\sim 10^{-4}$ Tesla) creates significant deflection over large distances ($\sim$ 100.000 km) thus providing a measurement of the charge of the primary particle.

The moon, by absorbing all particles, passing through it, will play a role similar to that of a collimator. The signal is given by the difference in counting rates with and without absorption by the moon. Figure A1 and A2 show schematically the principle of the experiment. The bending power of the earth moon spectrometer is $\int B.d\ell \simeq 100$ Tesla.meter. The magnetic field perturbations, mainly due to solar magnetic storms, stay usually within reasonnable limits ($\lesssim$ 10 %). The resulting deflection angle $\Delta\theta$, can be written as :

$$\Delta\theta = 30Z/E,$$

E in TeV is the incident particle energy, and Z, the electric charge in proton charge units. The moon apparent diameter, seen from the earth, is 10 mrad, introducing a comparable uncertainty on the cosmic ray initial direction. This value can be compared to $\Delta\theta \simeq 30$ mrad deflection for 1 TeV proton. The particles are detected through the Cerenkov radiation produced in the earth atmosphere.

The presence of the moon in the sky is necessary during the operation of the detector, as it defines the particle direction before deflection. But its presence is not compatible with the operation of ordinary Cerenkov telescopes. One has therefore to find a means of shielding the moon light, without depriving the detector from all the Cerenkov photons. The ozone layer, located as some 20 km altitude absorbs photons in the ultraviolet (UV) domain. UV photons originating from the moon or the stars cannot reach the ground, while Cerenkov UV photons produced below the ozone layer are not affected. The mean shower altitude being around $\sim$ 8 km, the presence of the ozone layer has nearly no effect on its development.

Cerenkov telescopes equipped with solar blind photo detectors, with good light detection efficiency in the UV vawelengths, but insensitive to visible light, can be operated in the presence of the moon.

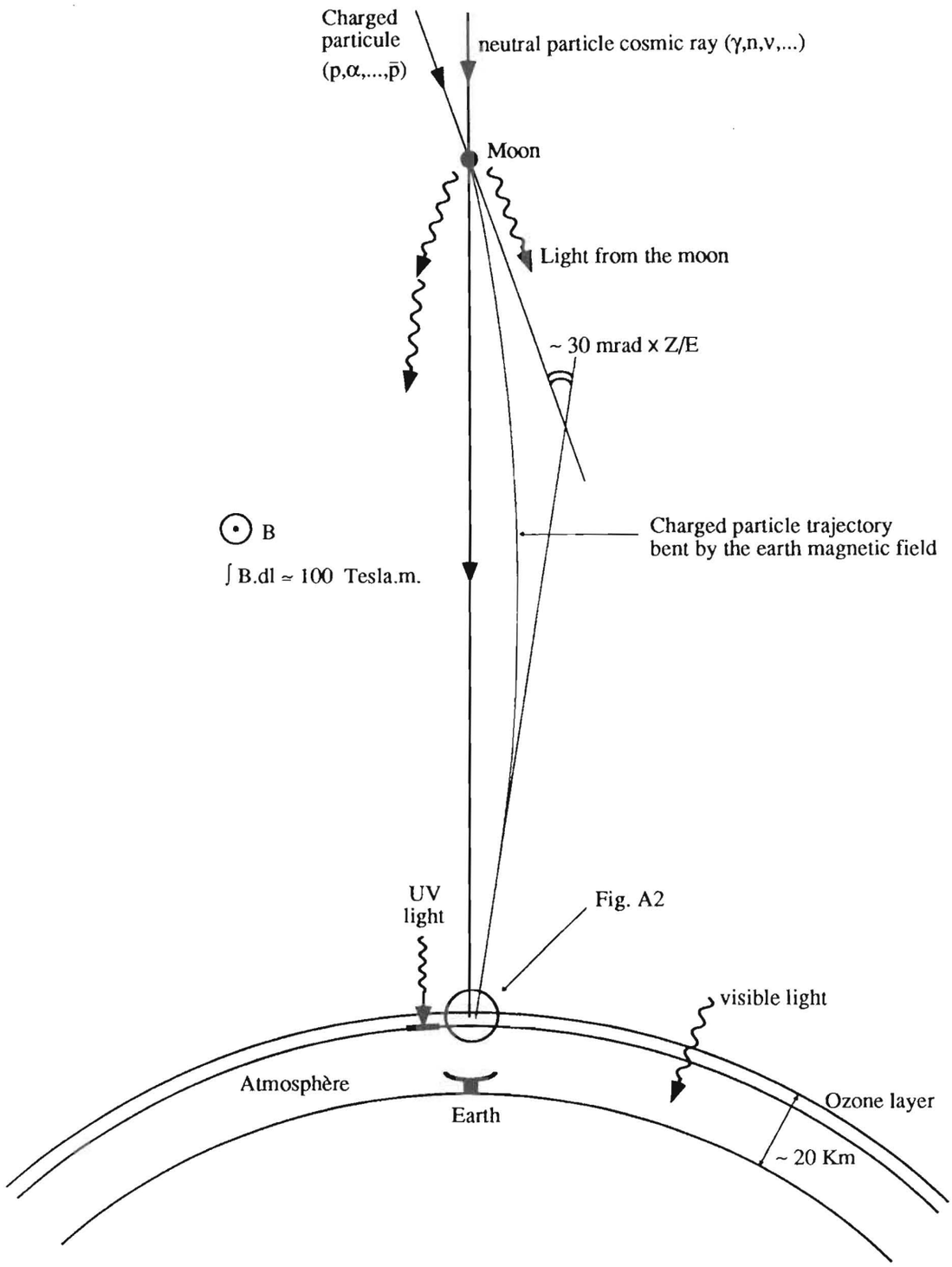

Fig A1 : Schematic representation of ARTEMIS spectrometer

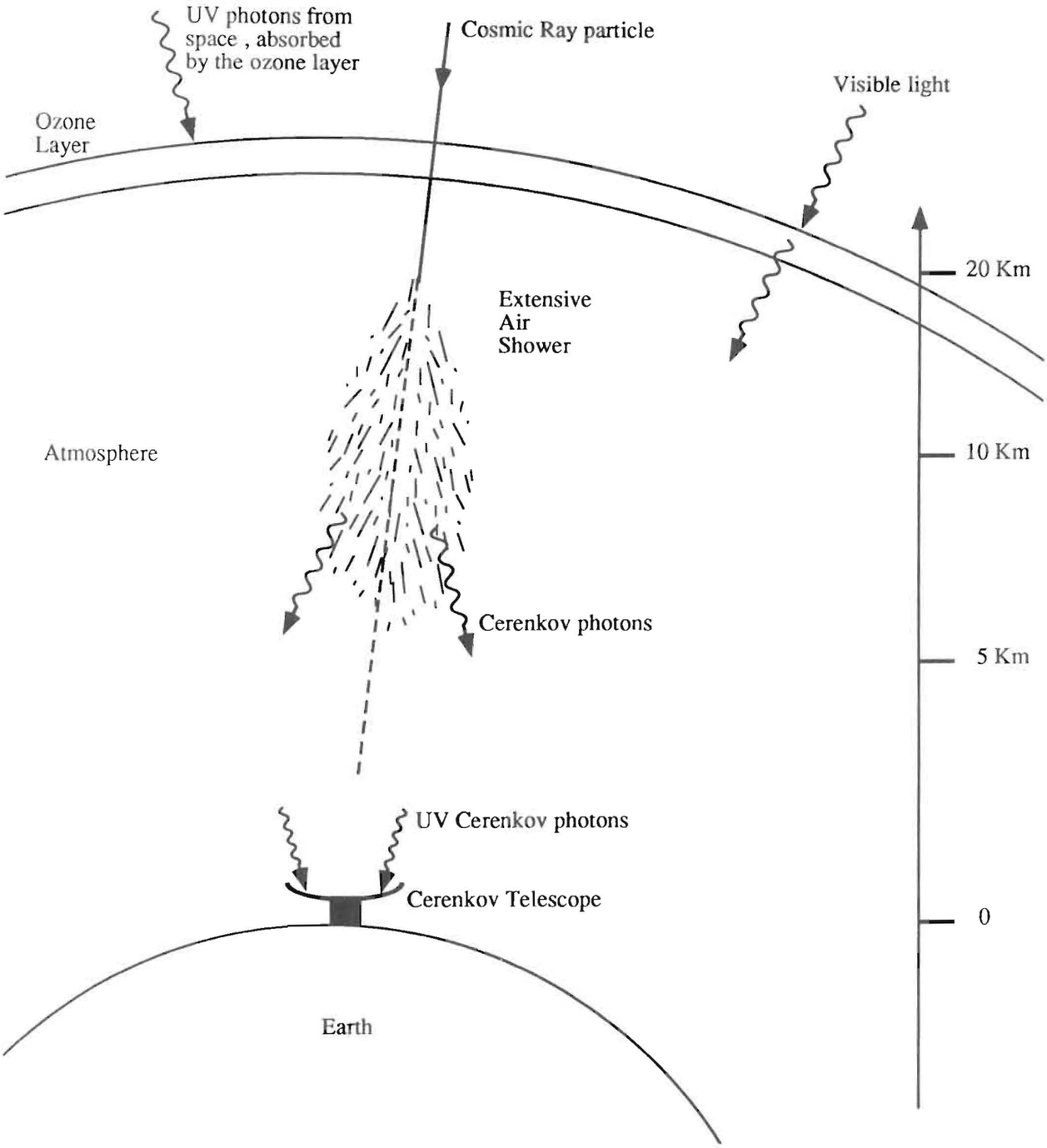

Fig A2 : Schematic representation of ARTEMIS spectrometer

Appendix B : MOCCA IMPLEMENTATION AT CC-IN2P3

The MOCCA (MOnteCarlo CAscade) atmospheric shower Montecarlo generator is available at CC-IN2P3 [3] on the IBM 3090 system running under VM-CMS. The generator code, developped by A.M. Hillas at Leeds University is written in Pascal. In order to facilitate the use of the CERN program library, we have written a small Fortran interface.

The operation of the generator is controlled through a datacard file, containing the run conditions and options, the primary particle type, energy, direction and position, as well as the Cerenkov telescope setup.

We have used the CERN HBOOK [4] Ntuple system to store the output results, mainly the collected Cerenkov photon characteristics. It is also possible to keep a complete trace of all secondary particles in the shower in Ntuples. The output data can then be analysed interactively using the PAW [5] program, or be further processed for detailed detector effect simulation for example.

B.1 Program source and command files

The list of files containing the programs as well as the command procedure with a short description is given below:

- MOCCA6 PASCAL : Generator Pascal code
- MOCCA FORTRAN : Fortran interface
- MOCCA EXEC : REXX [6] written command procedure for running the Montecarlo. The file contains the description of arguments and options.
- MOCCA DATA : Example of datacard set for MOCCA run
- MOCCA DATADESC : Complete description of datacards format and keywords

The HBOOK files produced by a MOCCA run can be processed using simple programs. The files NTLOOP FORTRAN and NTGRDZ FORTRAN contains examples of program capable of processing MOCCA output files. Two command procedures are available for this purpose.

- NTLOOP EXEC : REXX written command procedure for processing HBOOK files produced by a MOCCA run.
- TPNTLOOP EXEC : Command procedure for processing MOCCA output files stored on tape in VM tape dump format

[3] CC-IN2P3 : Centre de Calcul de l'Institut de Physique Nucleaire et de Physique des Particules
[4] HBOOK : Data handling, Statistical analysis and histogramming - CERN Program Library
[5] PAW : Physics Analysis Workstation - CERN Program Library
[6] REXX : Restructured Extended Executor Language - IBM VM/SP interpreter language

B.2 MOCCA datacard file

The simulation parameters are defined in a datacard file. Each data set is identified by a keyword followed by one or more blank separated arguments. By convention, all keywords begin with a '@' character, at a start of line. The datacard list has to be terminated by a '@END' keyword. There are mandatory and optional datacards. A complete description of the keywords can be found in the file MOCCA DATADESC.

The keywords '@PRIMARY' '@PRIMDIR' '@PRIMIMPACT' define the primary particle type, energy, direction and impact point. The various energy thresholds used in the simulation are controlled by the '@ROUGH', '@ESTOP' and '@THIN' datacards. The data associated with the '@THIN' keyword defines the thin sampling threshold discussed in section 3.3. The arguments following the '@RUNOPT' and '@OUTPUT' keywords define various simulation options and the list of tables included in the output listing file. The '@MIRROR' keyword controls the position, orientation and size of light collecting mirrors. Multimirror setup can be defined by using several '@MIRROR' datacards. The observation site altitude is defined by the '@OBSLEVEL' keyword and light attenuation parameters by '@LIGHT' keyword. The '@TRACSHOW' activates the storage of complete shower traces (all secondary particles) in the output HBOOK file.

B.3 Output Ntuples from MOCCA

The MOCCA results are stored in HBOOK Ntuples. The Ntuple 7550 contains summary information for generated showers. The characteristics of the collected photons are recorded in separate Ntuples [1..N], one per shower. Each collected photon has an entry in the shower Ntuple. The Ntuple variables with their content are listed below.

- MIRROR : The mirror number (0..N) which collected the photon.
- XDEG, YDEG : Cerenkov photon direction (in degrees)
- WT : Light emitting particle weight. Due to thin sampling (see section 3.3), secondaries may have weights larger than 1.The effective number of photons reaching the mirror is determined by WT. Photons emitted by muons are flagged using negative values of WT
- XA,YA : Photon impact position on the mirror, normalized to the mirror radius $-1 \leq XA, YA \leq 1$)
- TIME : Photon arrival time offset (in ns)
- EPAR : Emitting particle energy (in MeV)
- ZPAR : Photon emission altitude (in meters)

When the shower tracing option is activated, an Ntuple (numbered from 3000) containing the secondary particles is made for each shower traced. Each entry in these Ntuples corresponds to a track segment. The list of the corresponding Ntuple variables is given below.

* PTYP : Particle type, 0=Photon, 2=Neutrino, 4=Electron, 6=Muon, 10=Pizero, 14=Charged Pi, 24=Nucleon, 34=Nucleus - Negative numbers correspond to negatively charged particles
* PX,PY,PZ : Track position
* DIRX,DIRY,DIRZ : Track direction
* TKLEN : Track length, in meters
* E : Particle energy (in MeV)
* BETA : $\beta = v/c$
* WT : Particle weight

References

[1] M. Urban et al., ARTEMIS Proc. 22^{nd} Intern. Cosmic Ray Conf. (Dublin, 1991)

[2] M. Urban et al., Nuclear Physics B (Proc. Suppl.) **14B** (1990) 223-236

[3] P. Sokoloky, Introduction to Ultrahigh Energy Cosmic Ray Physics, Frontiers in physics, Addison-Wesley (1989)

[4] M.S. Longair, High Energy Astrophysics, Cambridge University Press

[5] T.C. Weekes, Phys. Reports **160** N° 1-2 (1988) 1-121

[6] B. Rossi, High Energy Particles, Prentice-Hall

[7] K.G. Gibbs, NIM **A264** (1988) 67-73

[8] R.M. Baltrusaitis et al., NIM **A264** (1988) 87

[9] M.F. Cawley et al., Proc. 19^{nd} Intern. Cosmic Ray Conf. (La Jolla, 1985) Vol. 3 p. 453

[10] T.C. Weekes, Proc. 17^{nd} Intern. Cosmic Ray Conf. (Paris, 1981) Vol. 8 p. 34

[11] A.M. Hillas, Proc. 17^{nd} Intern. Cosmic Ray Conf. (Paris, 1981) Vol. 8 p. 193

[12] A.M. Hillas, Proc. 16^{nd} Intern. Cosmic Ray Conf. (Kyoto, 1979) Vol. 6 p. 13

[13] F.W. Stecker, Nuclear Physics **B252** (1985) 25

[14] G. Basini, A. Morselli and M. Ricci, Riv. Nuov. Cim. **12** (1989) N°4 p. 1